Shared slides for

workshop on Challenges in high-latitude system dynamics

(http://cedarweb.vsp.ucar.edu/wiki/index.php/2018_Workshop:High_latitude_system_challenges)

to be held on Monday, 4 – 6 pm, 25 June in Mesa A/Hilton, Santa Fe.

https://docs.google.com/presentation/d/1IesIbs6bWYyQ5qoTG-AEQlGyuk22HsW7dtTXrGz46Vc/edit#slide=id.p

Please add questions, comments or discussion. This shared file will be kept open.

Link to upload slides:
https://docs.google.com/presentation/d/1IesIbs6bWYyQ5qoTG-AEQlGyuk22HsW7dtTXrGz46Vc/edit?usp=sharing

Introduction (3 minutes) Workshop structure – 5 minutes, 3 slides per presenter, all questions deferred to end, virtual discussion online

MIT Coupling

Hyunju Connor	Report from GEM FG on MIT coupling
Banafsheh Ferdousi	Relation between SAPS and neutral wind

Energy Input into IT

Bill Lotko	Alfvénic wave heating of IT
Olga Verkhoglyadova	Estimate of energy deposition by Alfvén waves
Cheryl Huang	High PF regions during magnetic storms
Ildiko Horvath	Coordinated PF and neutral density enhancements
Bob Robinson	Joule heating results from AMPERE
Ryan McGranaghan	Multi-scale FACs
Qingyu Zhu	Impacts of multi-scale FACs in GITM simulation of IT
Kristina Lynch	Data fusion: in situ plus imagery

Polar cap

Bea Gallardo	Automatic detection of polar cap boundary using DMSP, REGO observations
Andy Gerrard	Antarctic magnetometer measurements

Radar and rocket observations

Craig Heinselman	EISCAT 3D
Evan Thomas	SuperDARN measurements of ionospheric convection
Rob Gillies	Effect of polar cap patches on SuperDARN measurements

Workshop summary slide (2 minutes)

Questions for presenters and discussion (20 minutes)

Hyunju

GEM FG Report on MIT coupling

Hyunju Connor (UAF)

1. Brent Sadler: 2D IT model

Periodic soft electron precipitation produces neutral density enhancement above 400km altitude.

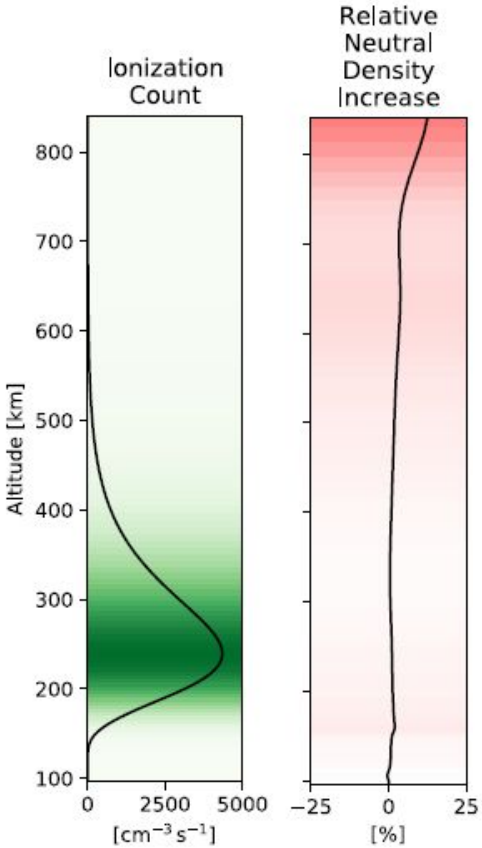

2. Hyunju Connor: OpenGGCM-CTIM MIT model

Sudden enhancement of Psw causes neutral density enhancement observed near the cusp.

DMSP and CHAMP Observation during Psw increase and IMF fluctuation

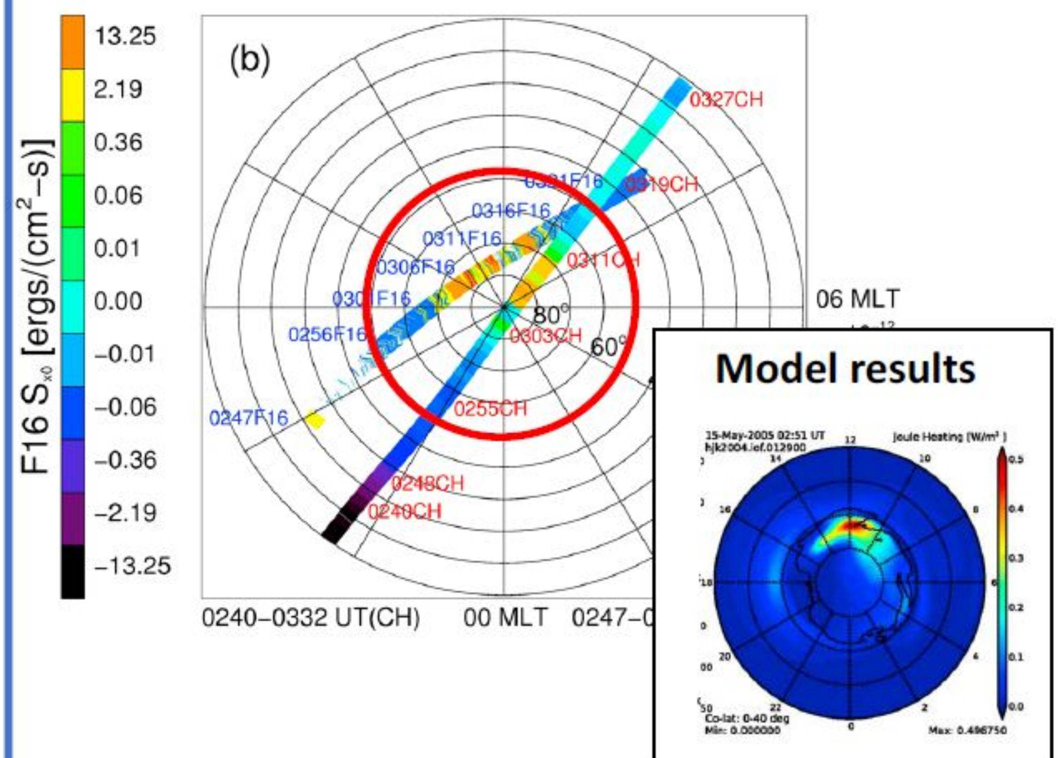

3. Doga Ozturk: SWMI-GITM one-way coupled model

Sudden compression and decompression of Psw produce opposite magnetospheric vortices, affecting FAC, Joule heating, ionospheric convection, etc.

Compression - Sudden Impulse (PI+):

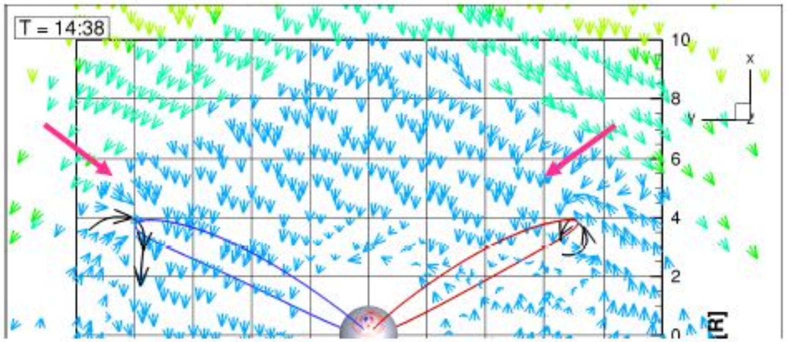

Decompression - Sudden Impulse (PI-):

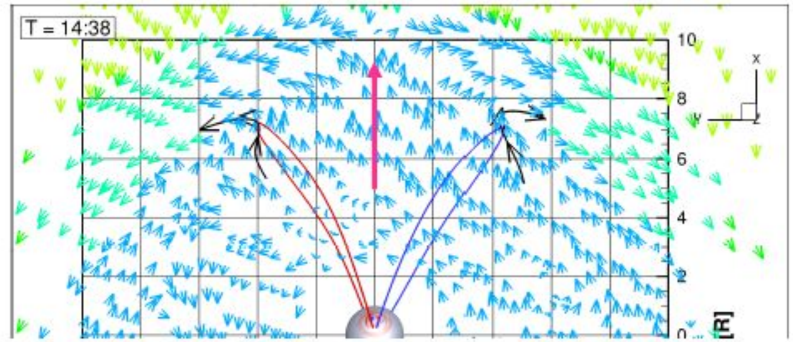

Stronger compression event on Mar 17, 2015

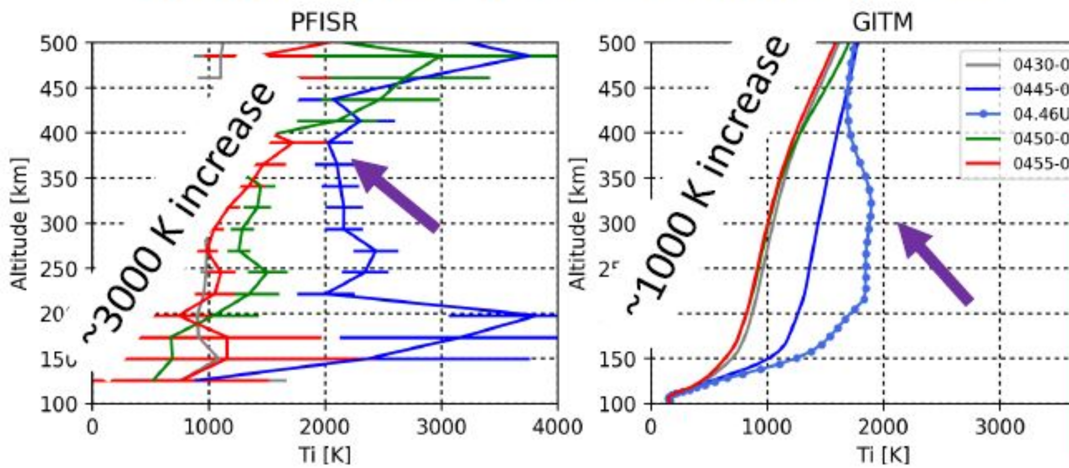

Ozturk et al.,

4. Kevin Pham: CMIT & CMIT-IPWM models

CMIT model does not show SW preconditioning effect in the MIT system. However, CMIT-IPWM one-way coupled model suggests that ion upflow/outflow can memorize the preconditioning effect and modify the MIT system.

CMIT

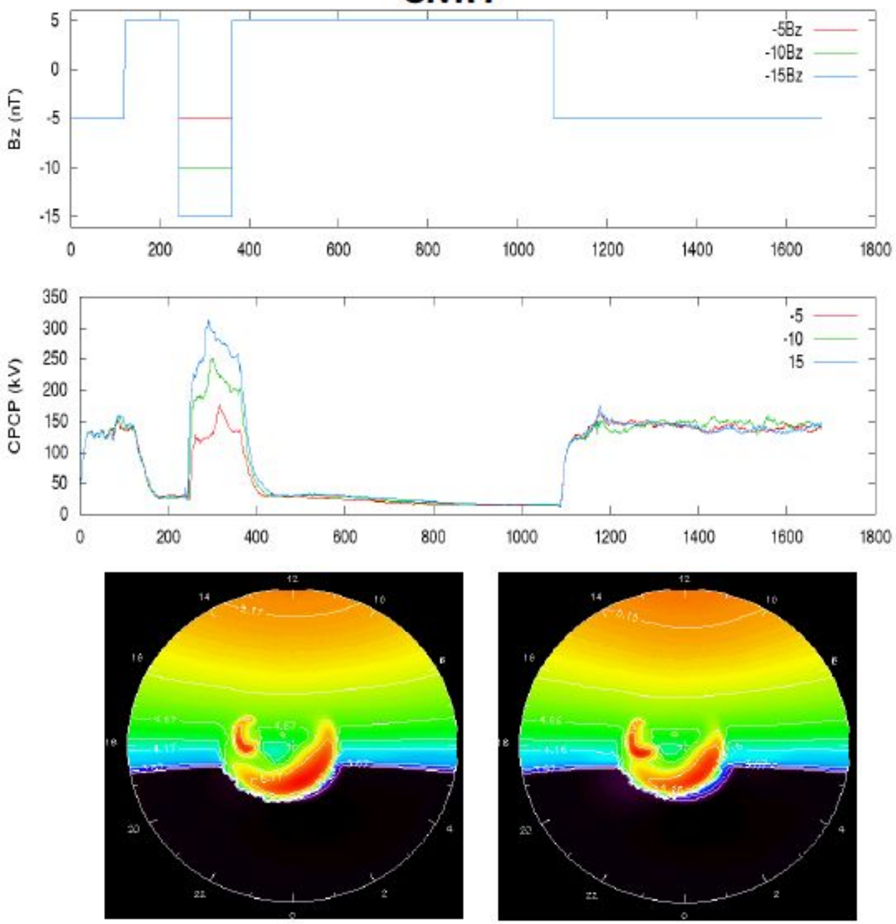

CMIT-IPWM

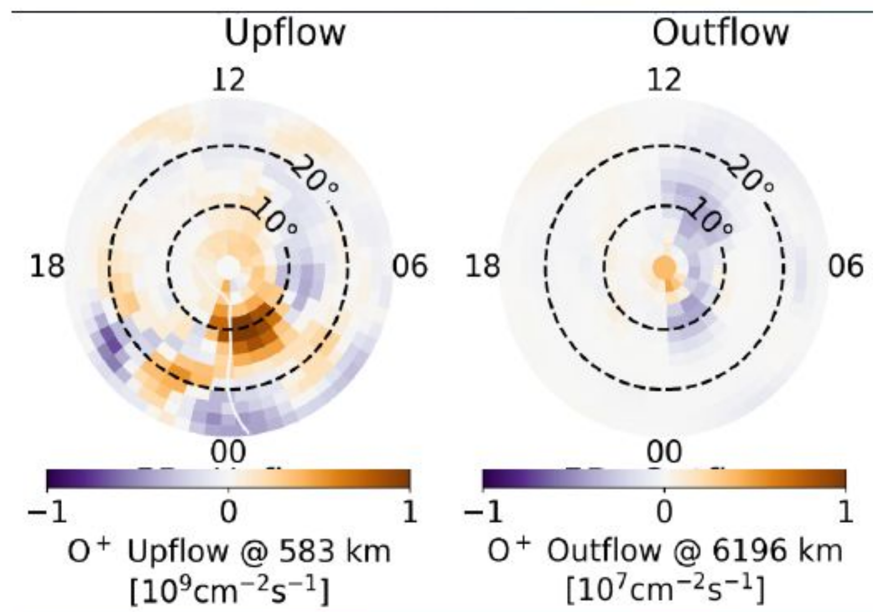

Bashi

Relation between SAPS and Neutral Wind (St Patrick's 2013 storm)

Observation (DMSP & GOCE) and Simulation (CTIPe-RCM) at Dusk (MLT=19)

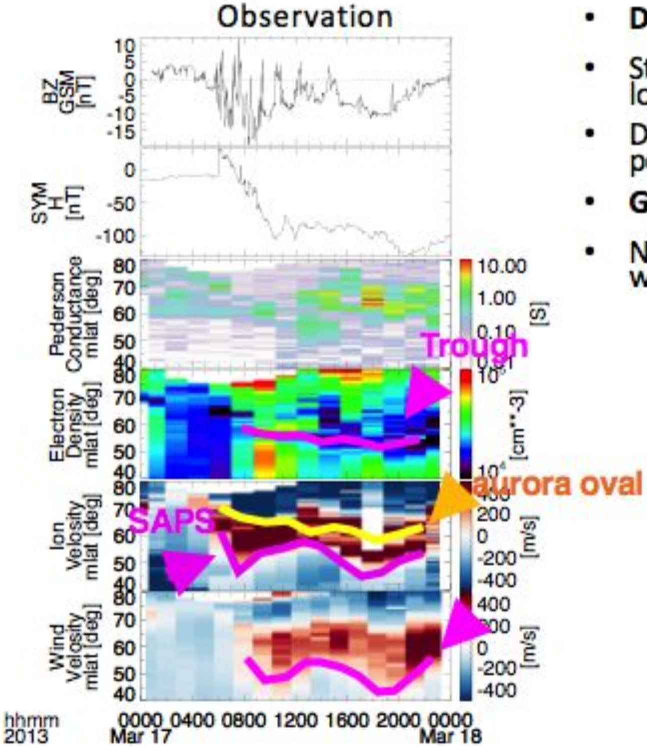

- **DMSP-18**
- Strong sunward ion flow and trough extend to lower latitudes (~45°).
- Double peak flow structure; the equatorward portion corresponds to SAPS.
- **GOCE**
- Neutral wind behaves similarly to the plasma flow with ~2 h delay.

Simulation successfully reproduced overall structure of SAPS and wind!

Question

What force drives the neutral wind in subauroral region?

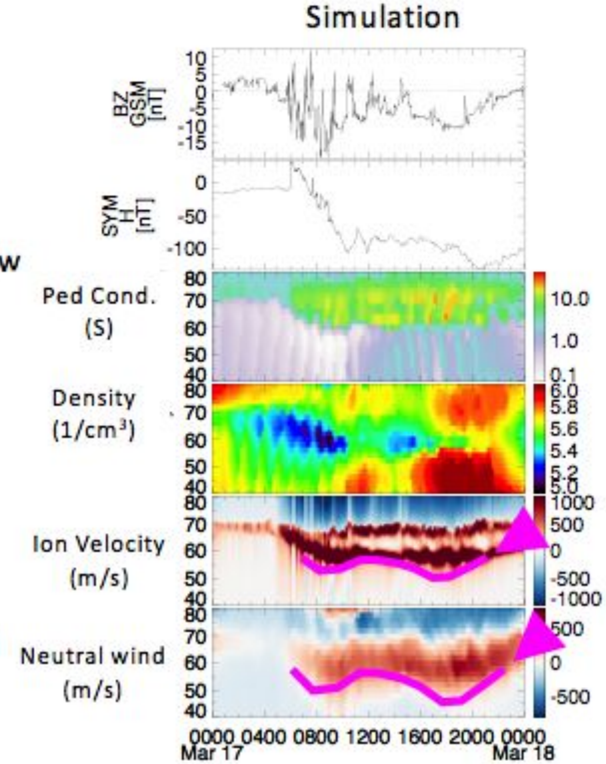

Authors: Banafsheh Ferdousi (bashi@bu.edu), Toshi Nishimura, Naomi Maruyama, Larry Lyons

Simulation Result: Force Term Analysis

Neutral Equation of Motion

$$\frac{\partial}{\partial t} V = \frac{1}{\rho} \nabla P + 2\Omega^{V} + \nu_{in}(V - U) + \frac{1}{\rho} \nabla(\mu \nabla V) + (V.\nabla)V$$

Pressure gradient | Coriolis | Ion drag | Viscosity | Advection

In Sunward direction

- Ion drag is the most dominant force.
- Coriolis force have contribution in lower latitude.
- The pressure gradient force generally acts against ion drag.
- The role of horizontal advection depends on latitude.

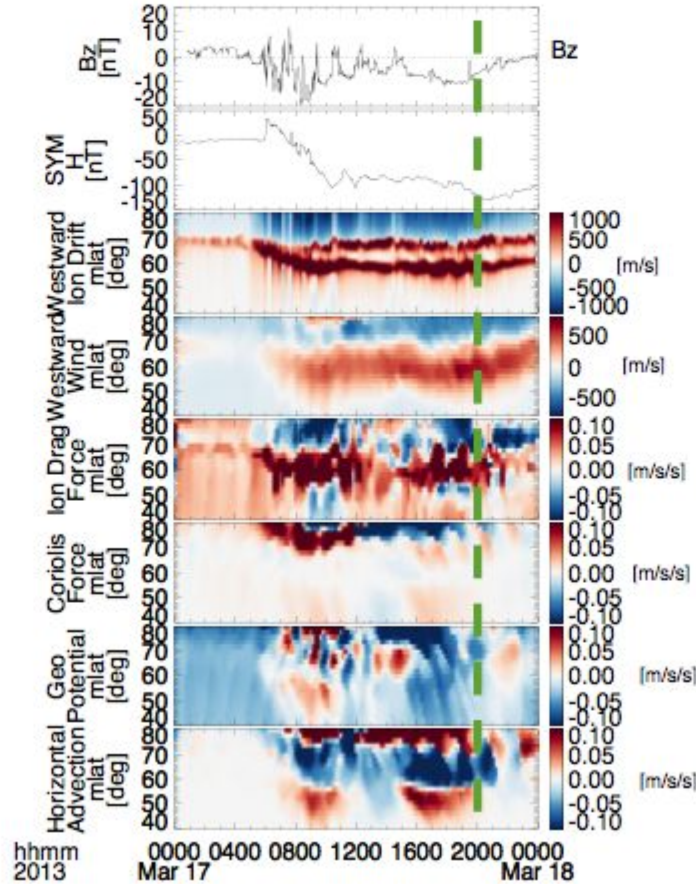

Simulation Result: Polar View of Force Term Analysis at T=20 UT

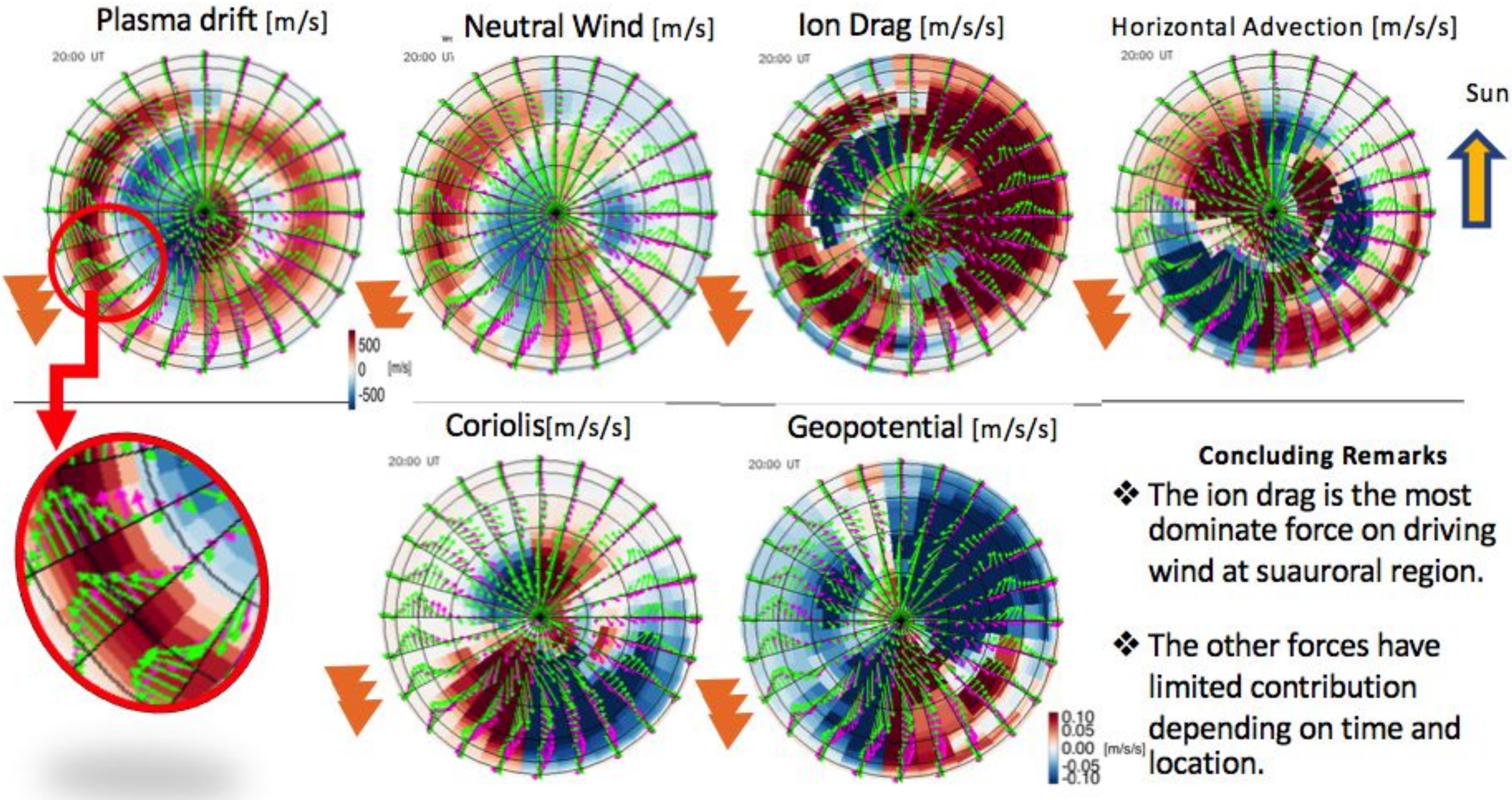

Concluding Remarks

- ❖ The ion drag is the most dominate force on driving wind at suauroral region.
- ❖ The other forces have limited contribution depending on time and location.

Bill Lotko

Bill Lotko, wlotko@dartmouth.edu

Simulation Schematic

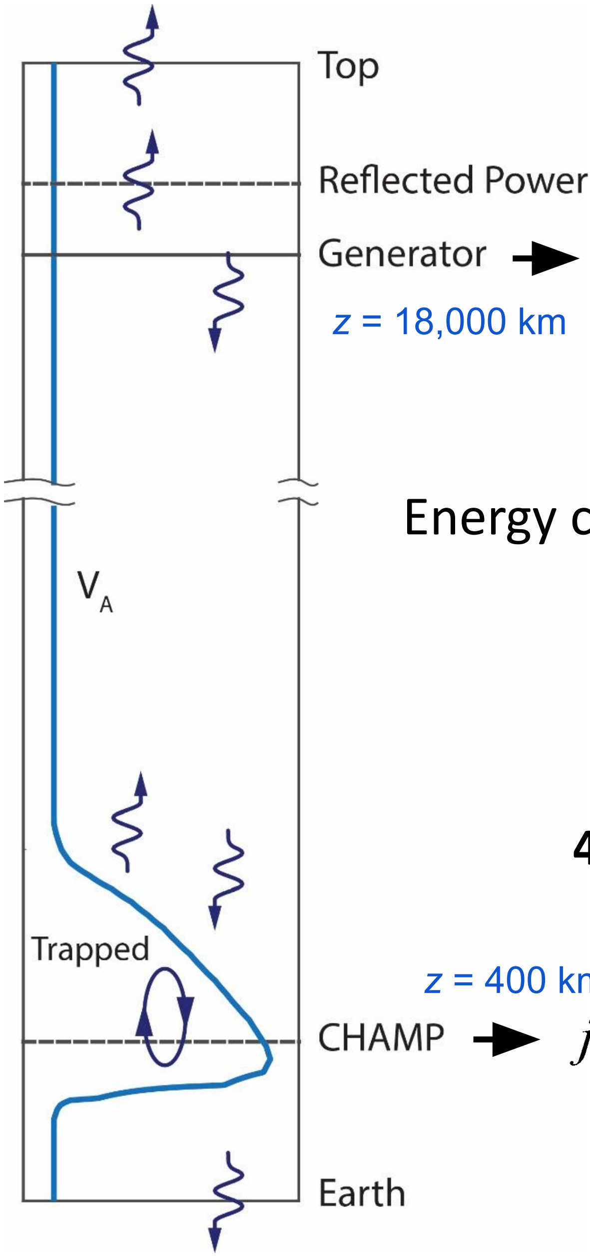

CUSP IONOSPHERE

Generator → Downward propagating Alfvén wave
z = 18,000 km (adjust amplitude to match CHAMP FAC at 400 km)

Energy conservation: $P_{Gen} = P_{Ref} + P_{Abs} + P_{Trans}$ (with P_{Trans} struck through)

P_{Abs}: Joule + Ohmic

P_{Trans}: Negligible

Launch Alfvén waves at high altitude

Diagnose interaction with ionosphere

40×40 modes | 0.05 < f < 2Hz | 0.5 < $\lambda_\perp$ < 20km

CHAMP → z = 400 km

$$j_z(x,z,t) = \sum_{m=1}^{40}\sum_{n=1}^{40} j_{m,n}(z)\cos(2\pi m x/\lambda_{max} + \theta_m)$$

(with x struck through and replaced by $v_s t$)

$$\times\cos(2\pi n t/\tau_{max} + \theta_n + \phi_{EB})$$

Absorbed Power vs Altitude

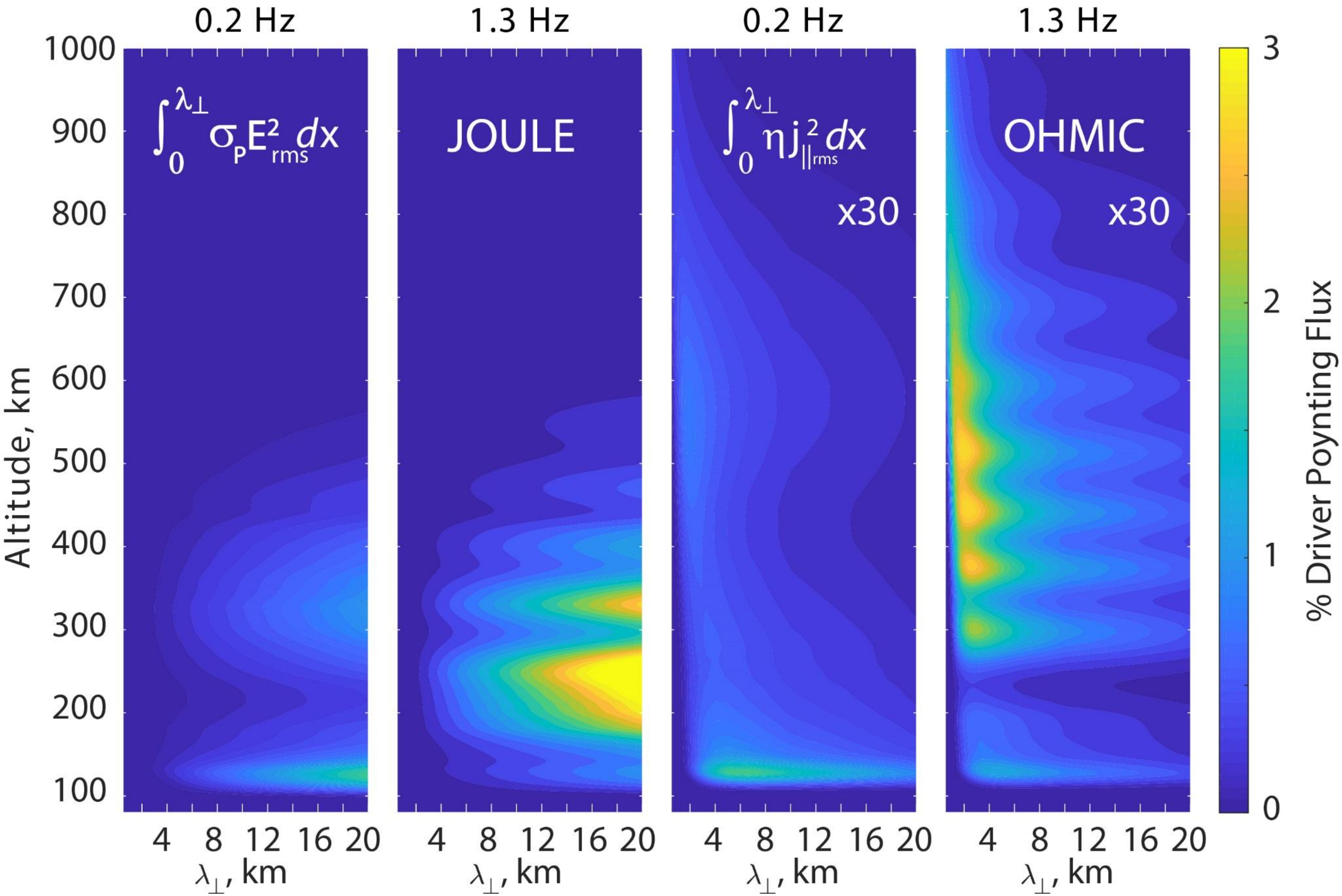

Fields at 400 km | Heating Rate vs Altitude

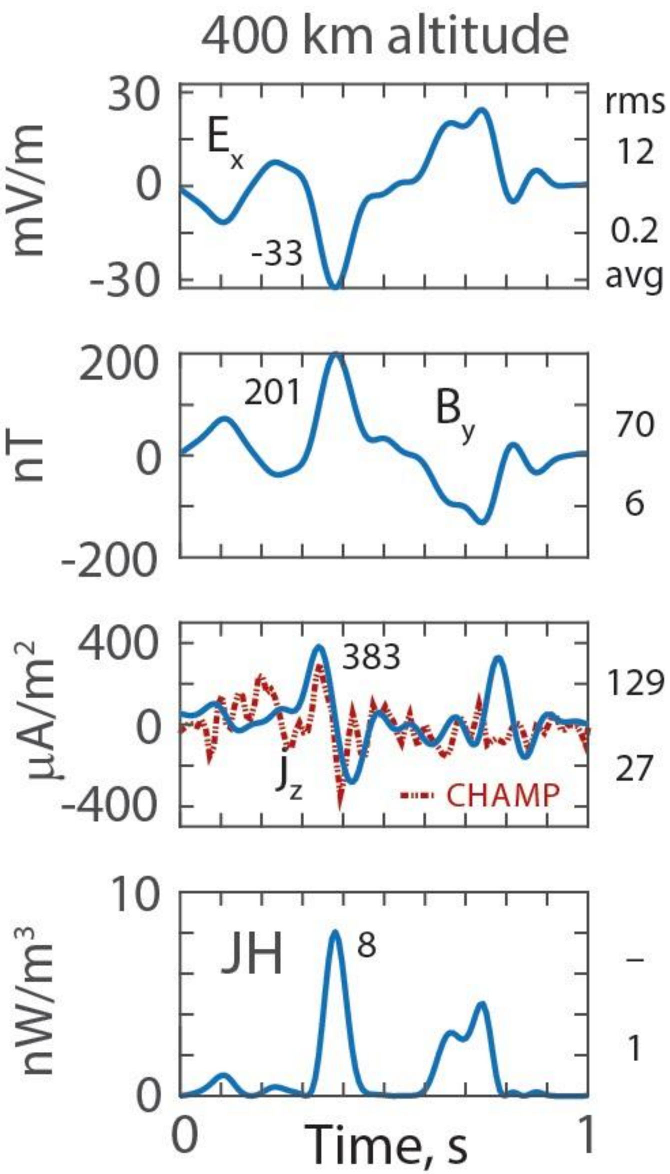

E_x, B_y comparable to DE-2 at 312 km (*Ishii* 1992)

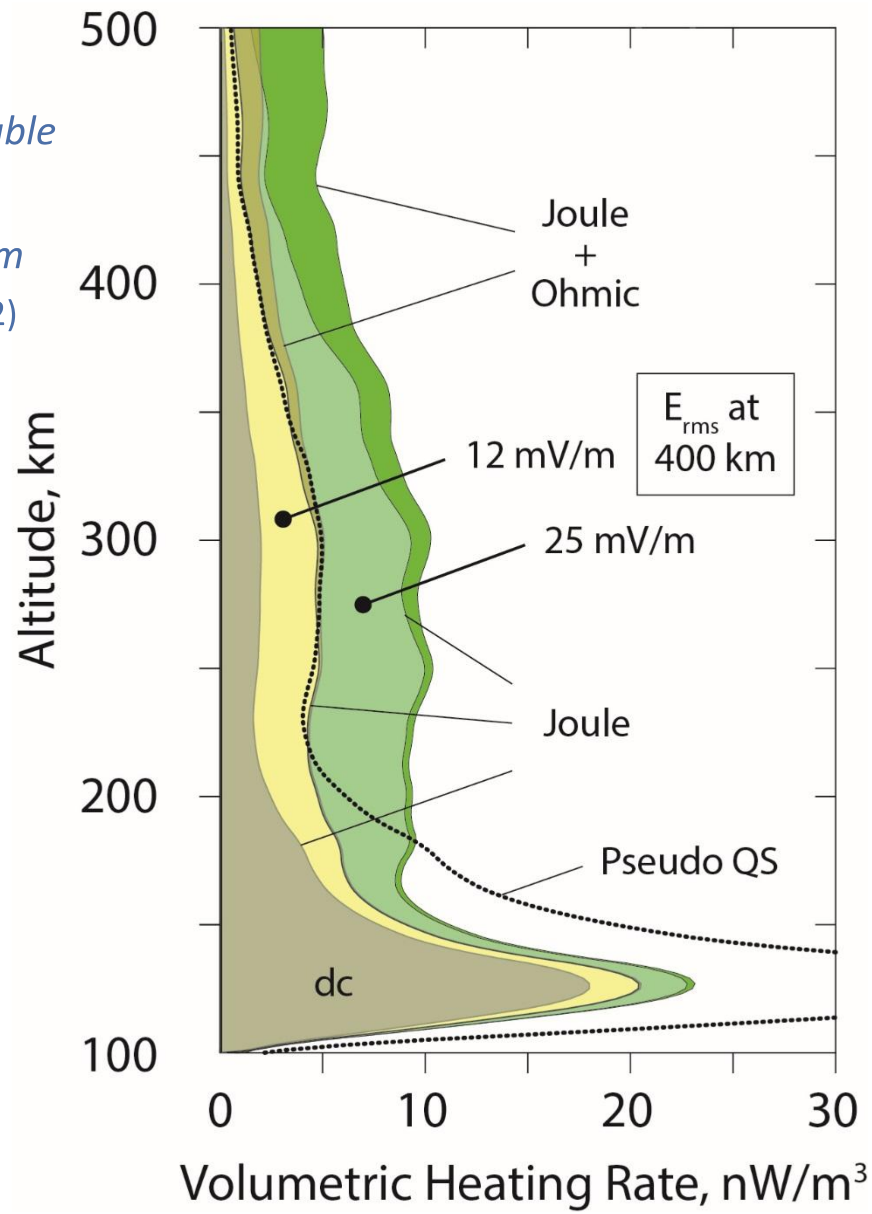

Olga

Estimate of energy deposition by Alfvén waves in the IT

O. P. Verkhoglyadova, X. Meng, A.J. Mannucci (1), R. McGranaghan (1, 2)

[1]Jet Propulsion Laboratory, California Institute of Technology, Pasadena, CA;
[2]University Corporation for Atmospheric Research (UCAR), Boulder, USA

- Recent ground-based and spacecraft observations indicate the importance of dynamic ionospheric response to external driving, and the existence of transient and multi-scale plasma features in the high-latitude IT (Huang and Burke, 2004; Semeter et al., 2010; Lyons et al., 2016; Huang et al., 2016; McGranaghan et al., 2017+)

- ULF/Alfvén waves are important contribution to electromagnetic energy flow from the magnetosphere to the high-latitude ionosphere during geomagnetically active periods (Keiling et al., 2003; Lotko, 2004, 2007; Chaston et al., 2005; Hatch et al., 2016; Miles et al., 2018; Pakhotin et al., 2018+)

The relative efficiencies of Alfvén wave dissipation during quiet-time and storm

$$\langle \frac{\partial W}{\partial t} \rangle_T = \tilde{\sigma}_P \langle |\boldsymbol{E}_\perp|^2 \rangle_T \qquad \tilde{\sigma}_P = \epsilon_0 \sum_\alpha \frac{\nu_\alpha \omega_{p\alpha}^2 (q_\alpha^2 + 2\omega^2)}{q_\alpha^4 + 4\omega^2 \nu_\alpha^2}, \quad \tilde{\sigma}_{||} = \epsilon_0 \sum_\alpha \frac{\nu_\alpha \omega_{p\alpha}^2}{\omega^2 + \nu_\alpha^2},$$

$$q_\alpha^2 = \nu_\alpha^2 - \omega^2 + \omega_{c\alpha}^2.$$

GITM modeling of the 13-14 October 2016 storm

Changes in the Pedersen conductivity due to waves at 60° lat and 12LT

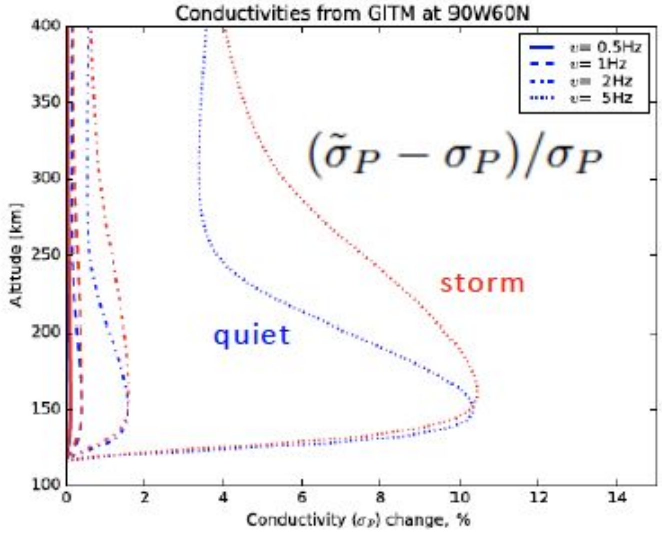

$$\kappa = \frac{Q_w}{Q_s} = \frac{\tilde{\sigma}_P}{\sigma_P} \cdot \frac{\langle |E_{\perp w}|^2 \rangle_T}{|E_{\perp s}|^2} \approx 1.1 \cdot \frac{\langle |E_{\perp w}|^2 \rangle_T}{|E_{\perp s}|^2}$$

$E_{\perp s}$ quasi-static field

Table 1. Horizontal electric field estimations from GITM at 60° latitude.

Time	Quiet time value, mV/m	Storm time value, mV/m
12 LT (18 UT)	0.25 (11 Oct.)	46 (13 Oct.)
20 LT (06 UT)	0.60 (12 Oct.)	30 (14 Oct.)

$E_{\perp w} \sim 20 - 40\ mV/m$ Alfvén wave field

Alfvén wave contribution to storm energy deposition as compared to static Joule heating:

$\kappa \approx 30\ \%$

Conclusions

- An analytical expression for energy deposition by propagating Alfvén waves in the collisional ionosphere-thermosphere is derived.
- The relative efficiency of energy deposition rate of Alfvén wave (up to 5Hz in. frequency) to static field is estimated to be ~10% at high latitudes and below 250 km altitude.
- We show that Alfvén wave energy deposition can reach about 30% of the value of static Joule heating during a strong storm.
- **This effect carries important implications for ionospheric dynamics, especially for density enhancement in the daytime cusp, heating in the vicinity of auroral arcs and ion outflow.**

Verkhoglyadova et al, JGR, 2018; https://doi.org/10.1029/2017JA025097.

Cheryl

High Poynting Flux Regions

Cheryl Huang[1], Yanshi Huang[2], Tom Sotirelis[3]

[1]Air Force Research Laboratory; [2]Harbin Institute of Technology; [3] Applied Physics Laboratory

There are 14 moderate storms in our DMSP Poynting flux database.

- **Select NH passes at high latitudes on the dayside.**
- **Use 20 mW/m^2 as our working definition of high PF.**
- **Determine the regions where this level of PF occurs, based on DMSP particle precipitation measurements, using the APL boundary identification algorithm**

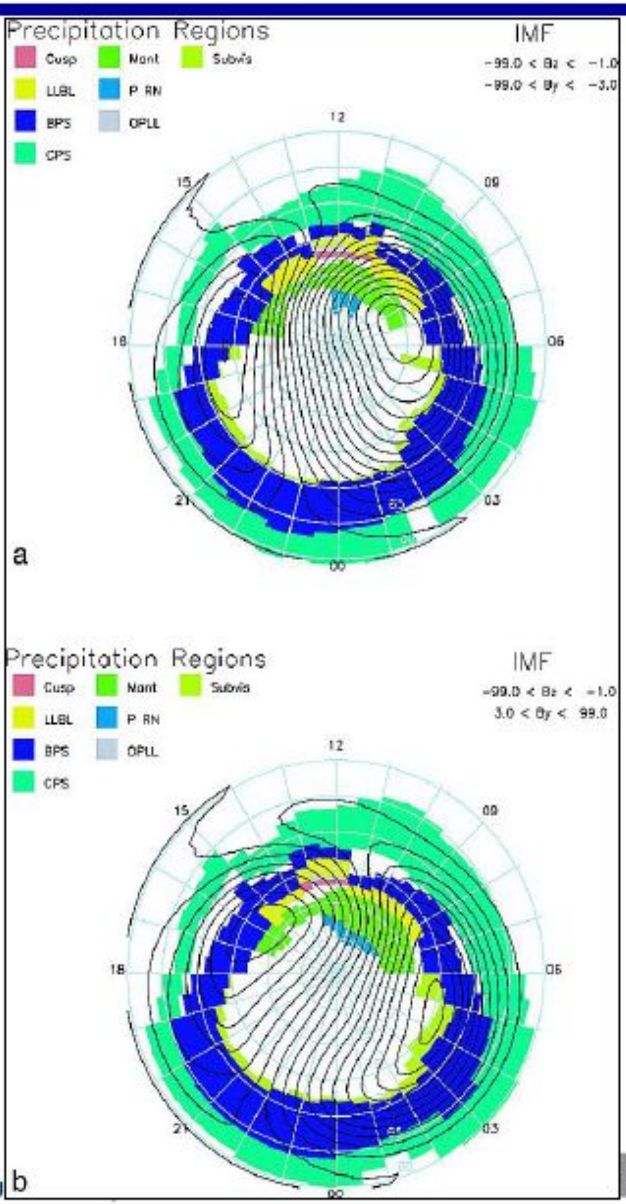

Boundary definitions based on particle precipitation [Newell et al., 2004]

High Poynting flux and particle precipitation

Example: DMSP F18 DOY 217, 2011, 1954 UT

$S_x > 20$ mW m^{-2}

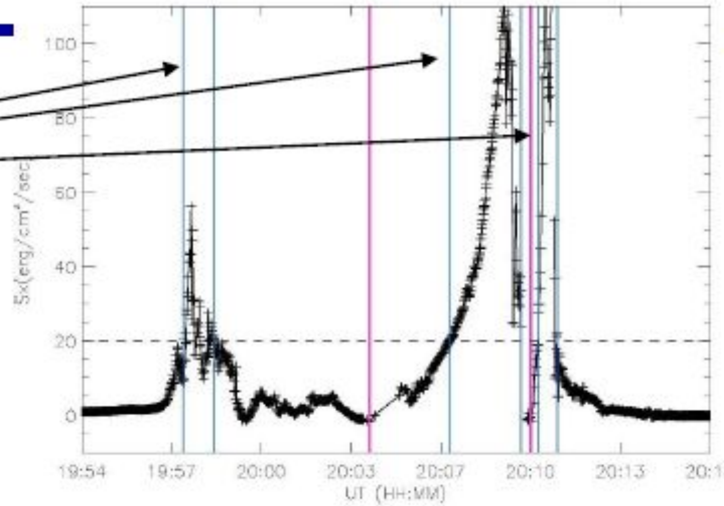

For this pass, the high PF regions correspond to: (1) nightside; (2) polar cap; (3) LLBL, CPS, cusp, BPS

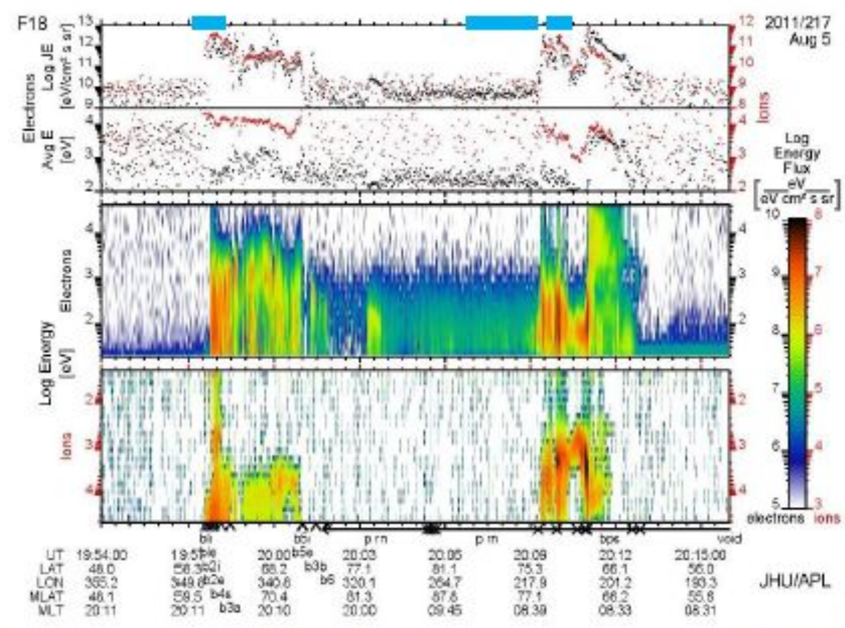

Results of high PF study

14 storms; 279 high PF boundary regions identified

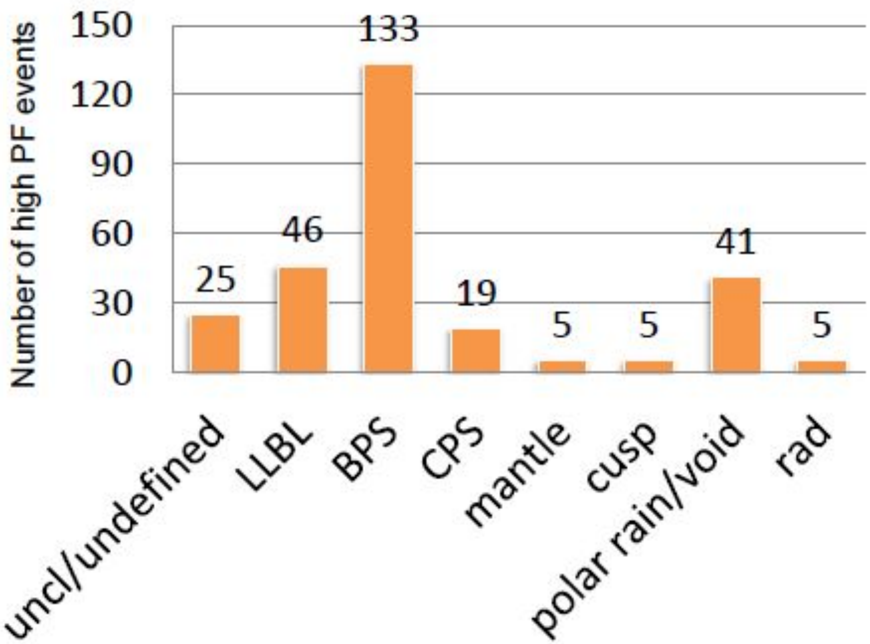

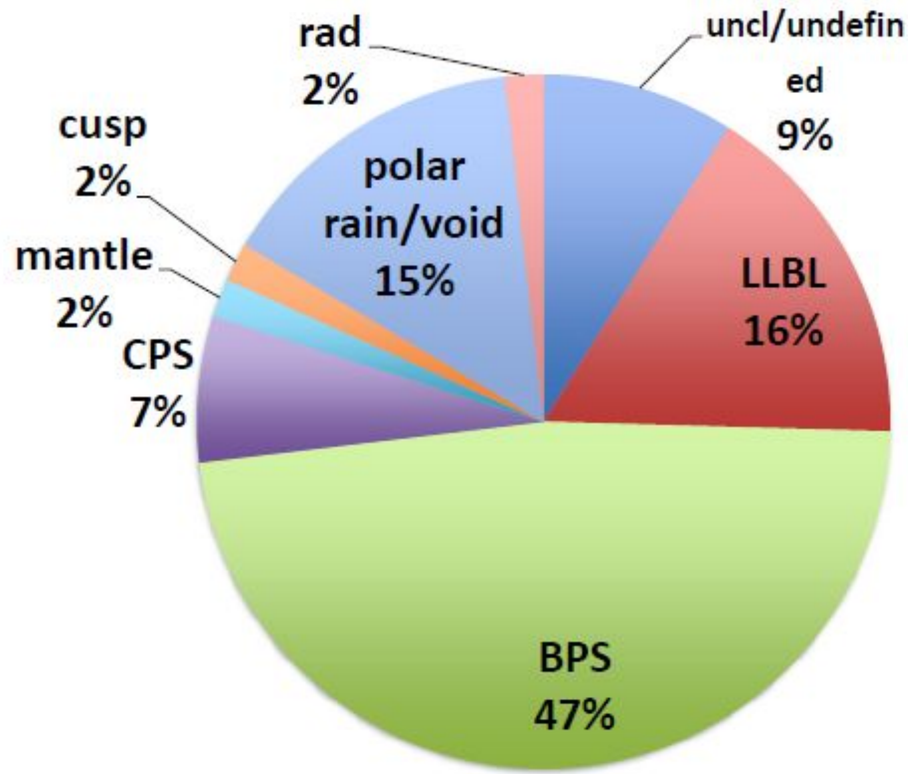

Roughly half the high PF events occur in the BPS – note this is not the same as saying that half the PF occurs in the BPS. But the *entire dayside ionosphere at high latitudes* is affected by solar wind merging.

Not shown: There appears to be little correlation between particle precipitation and high PF occurrence, i.e. high PF can occur with weak precipitation (low energy and/or low number flux) and vice versa. High energy input is *not correlated* with high conductivity.

Ildiko

Coordinated Poynting Flux and Neutral Density Enhancements During the 17 January 2005 Geomagnetic Storm

Ildiko Horvath and Brian Lovell, The University of Queensland, Australia

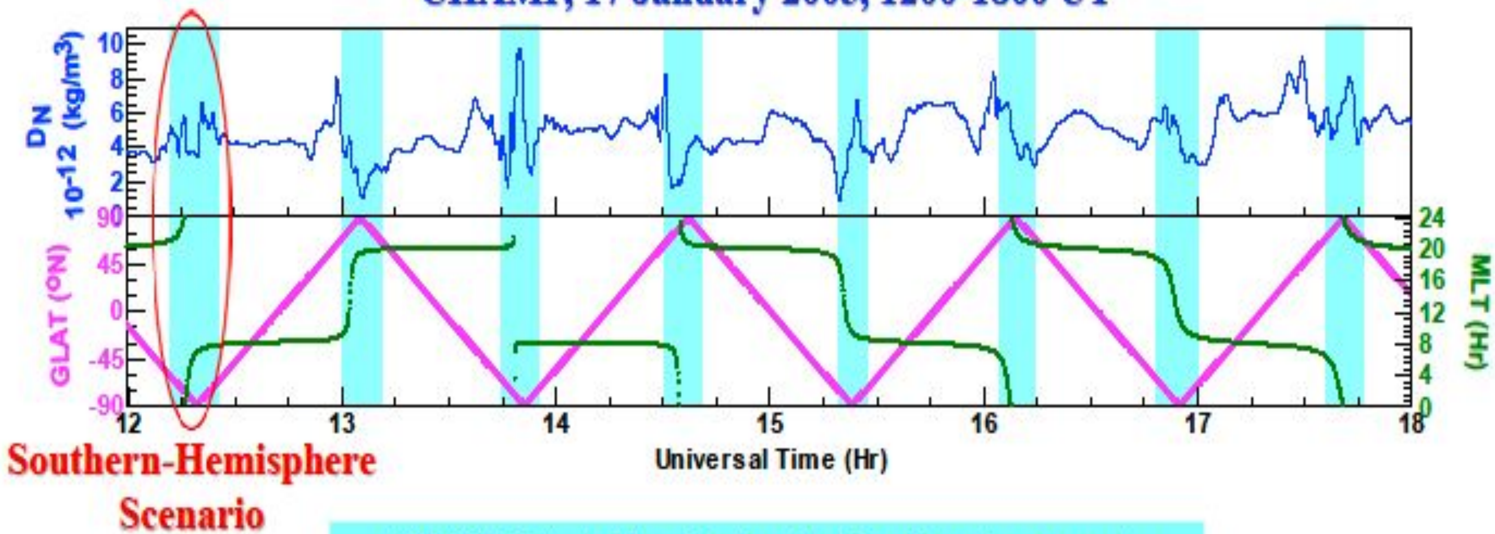

CHAMP detected localised neutral density enhancements over the northern and southern cusp and polar cap regions.

This study's aims are to find out:

- how the Poynting flux, derived from DMSP data, became deposited and varied over the auroral and polar cap regions, and
- how the thermosphere responded to these Poynting flux depositions.

Correlated CHAMP & DMSP F15 Polar Cross Sections

1)
Localised morning (7-8 MLT) density peaks developed within FC-1 & FC-3.

2)
FC-1 & FC-3 signatures are in zonal winds.

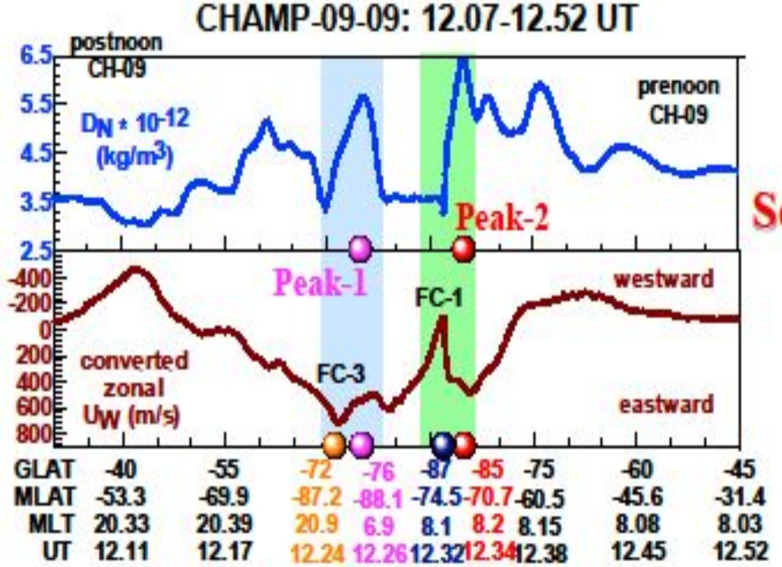

Southern-Hemisphere Scenario

3)
FC-1 & FC-3 signatures are in zonal drifts.

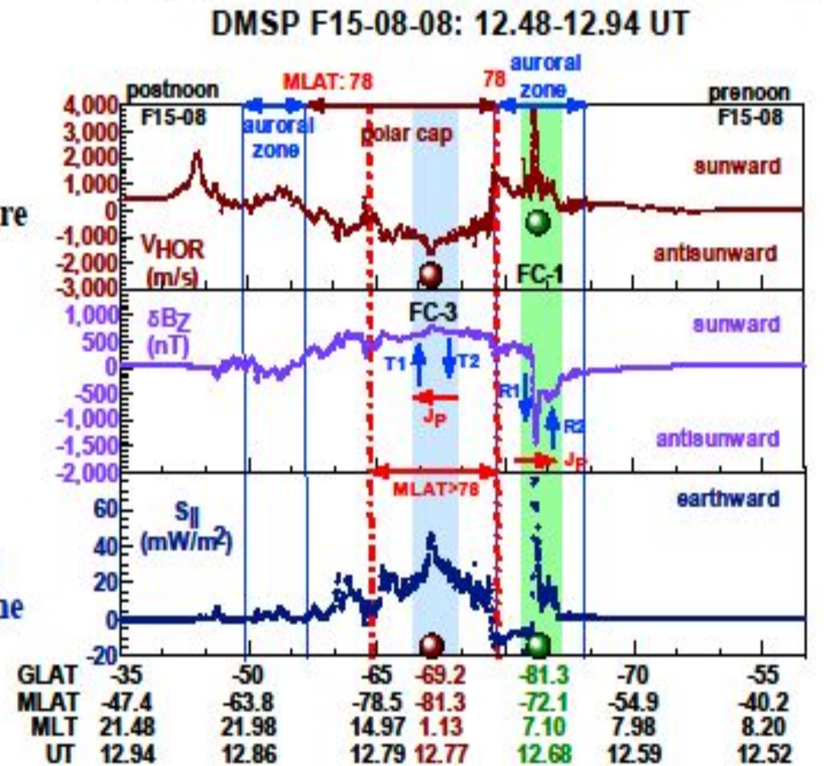

4)
In FC-1 (Region) R1-R2 FACs and in FC-3 (Tail) T1-T2 FACs connect via ionospheric Pedersen currents (J_P) ***[Sandholt & Farrugia 2012]*****.**

5)
The earthward Poynting flux peaked locally within FC-1 and FC-3 and became elevated within the MLAT>78 region of the polar cap.

Southern-Hemisphere Scenario:
Correlated CHAMP and DMSP F15 Polar Plots

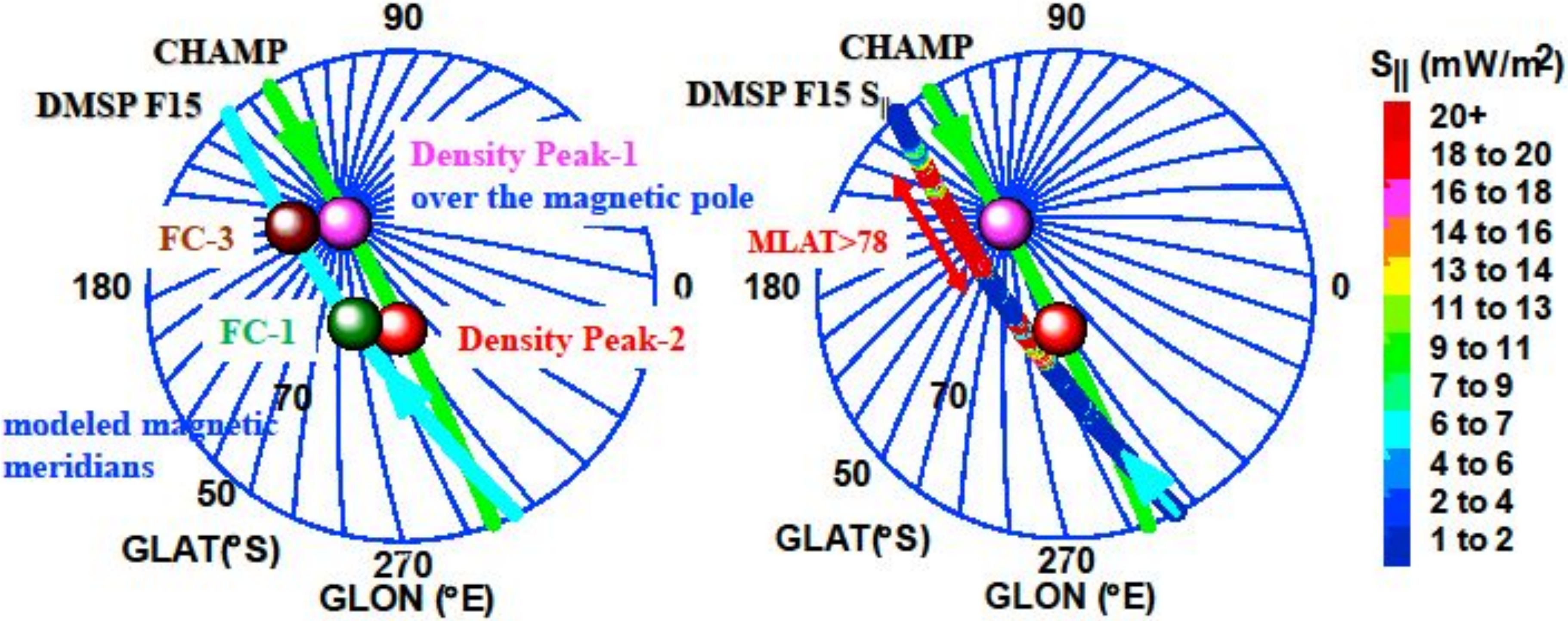

Conclusions

(1) Correlated CHAMP and DMSP F15 measurements demonstrate the coordinated enhancements of earthward Poynting flux ($S_{\|}$) and neutral density within FC-1 & FC-3.

(2) Electromagnetic energy ($S_{\|}$) input via flow channel was the primary driver of the development of the localized neutral density peaks investigated.

(3) The central polar cap (MLAT>78 region) was the main region of electromagnetic energy deposition during this scenario.

Bob Robinson

Bob Robinson, Catholic University

AMPERE Measurements of Field-Aligned Currents

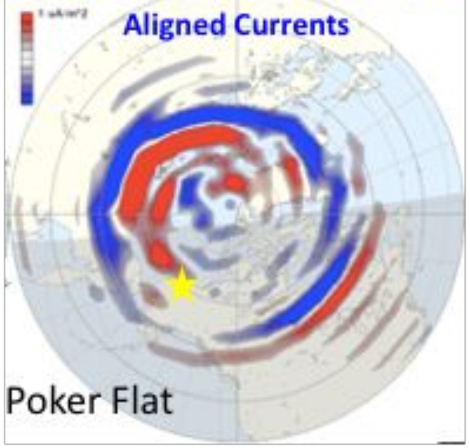

\+

Poker Flat Incoherent Scatter Radar measurements of ionospheric electron densities

By statistically relating AMPERE field-aligned currents to conductivities and energy flux calculated from PFISR electron density measurements, we can self-consistently calculate energy flux, electric fields, currents, and Joule heating directly from AMPERE FAC maps.

$$J_{\|} = \nabla \cdot (\bar{\bar{\Sigma}}\bar{E})$$

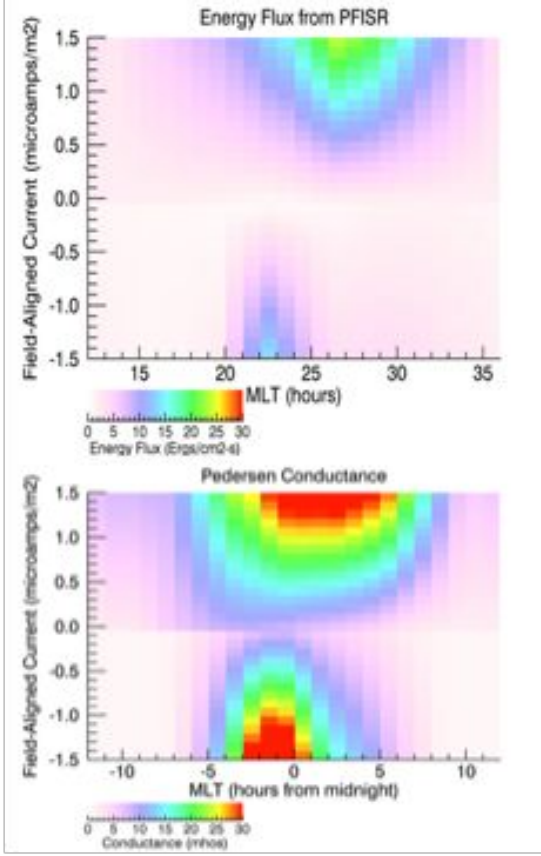

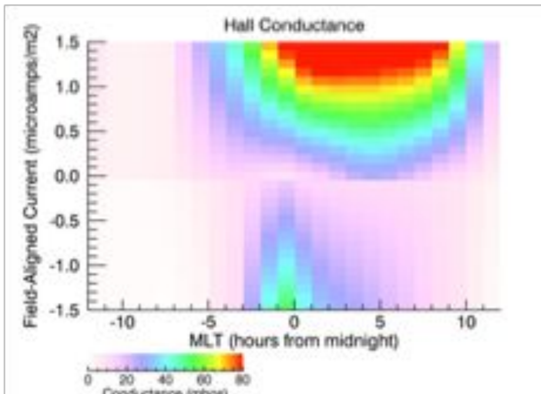

- Joule heating is localized and impulsive, and dominates energy input from precipitating particles during geomagnetically active periods.
- Largest Joule heating is found in the MLT sectors where the field-aligned current is well correlated with conductance.
- Impulsive Joule heating events coincide with loss of energy from ring current as determined from Dst.

Joule heating (black) and energy flux from precipitating particles (red) vs polar cap potential
50 geomagnetically active days

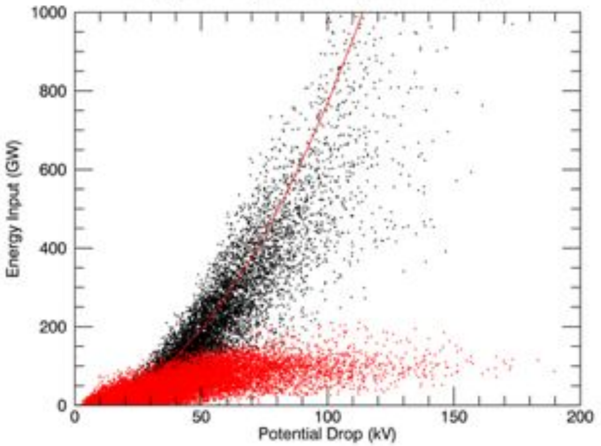

MLT Distribution of Joule Heating
> 50 ergs/cm²-sec
24 Geomagnetically Active Days

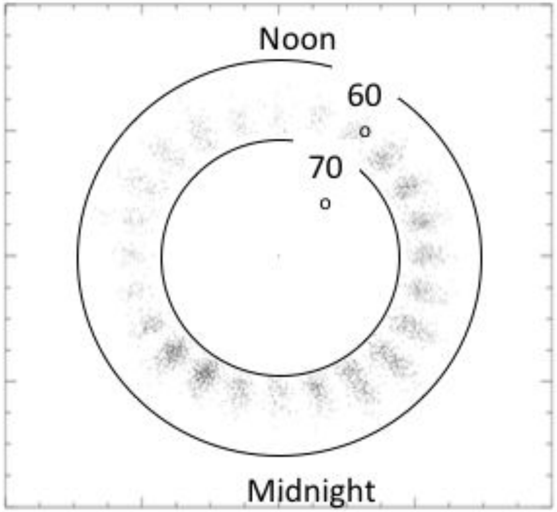

Total energy Input and Dst
5 April 2010

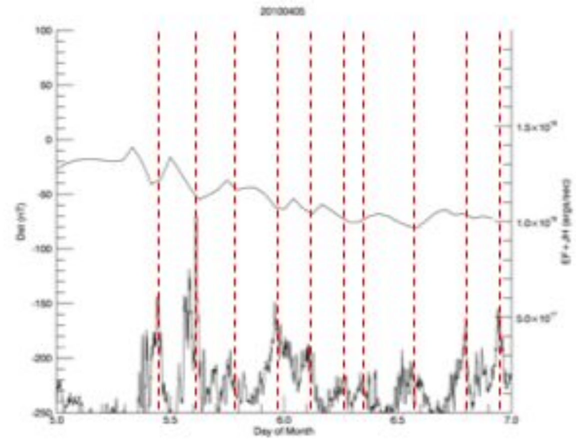

The localized and impulsive nature of the Joule heating events is a result of the increase in conductivity with field-aligned current, which makes the magnetosphere-ionosphere current system a variable resistant circuit subject to runaway current conditions as the electric field increases.

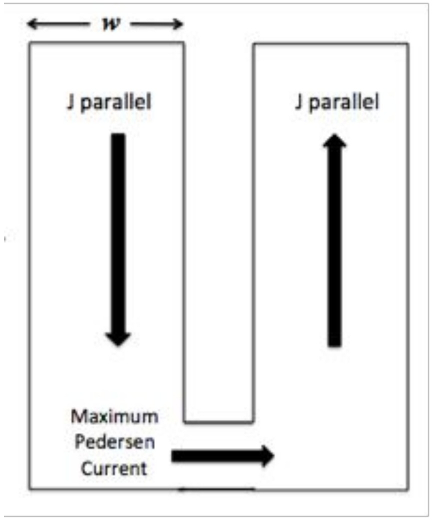

$$J_P = \Sigma_P \bar{E}$$

$$\Sigma_P = \Sigma_o + mJ_\parallel$$

$$J_P = \Sigma_o \bar{E} + mJ_\parallel \bar{E}$$

$$J_{P_{max}} = wJ_\parallel$$

$$J_{P_{max}} = \Sigma_o \bar{E} + mJ_{P_{max}} \bar{E}/w$$

$$J_{P_{max}} = \frac{\Sigma_o \bar{E} w}{(w - m\bar{E})}$$

$$JH_{max} = \frac{\Sigma_o \bar{E}^2 w}{(w - m\bar{E})}$$

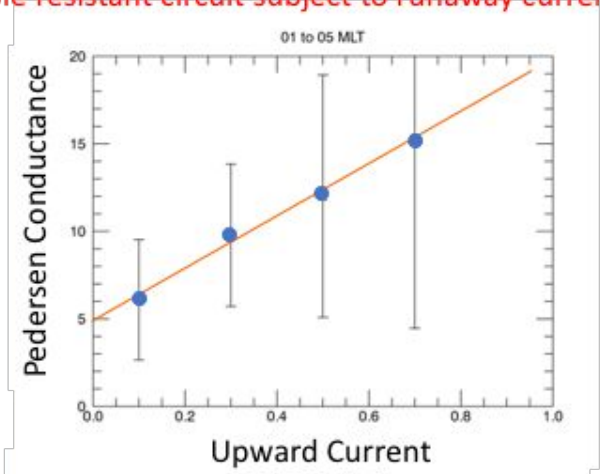

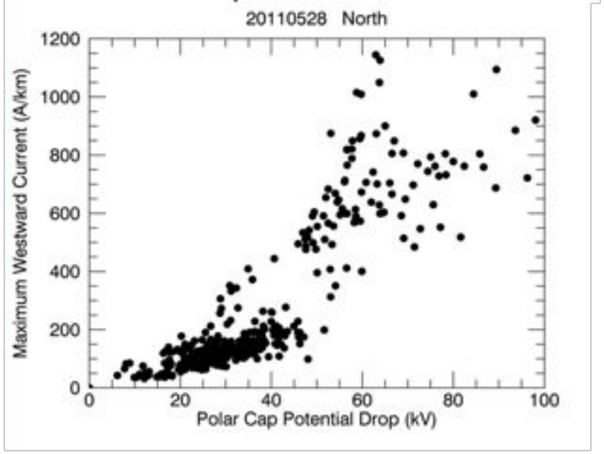

Ryan

Large-scale model

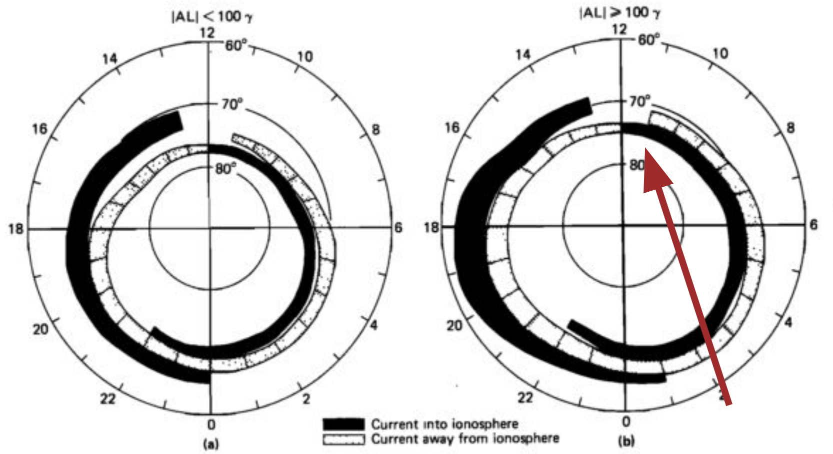

Iijima and Potemra [1978]

Small-scale reality

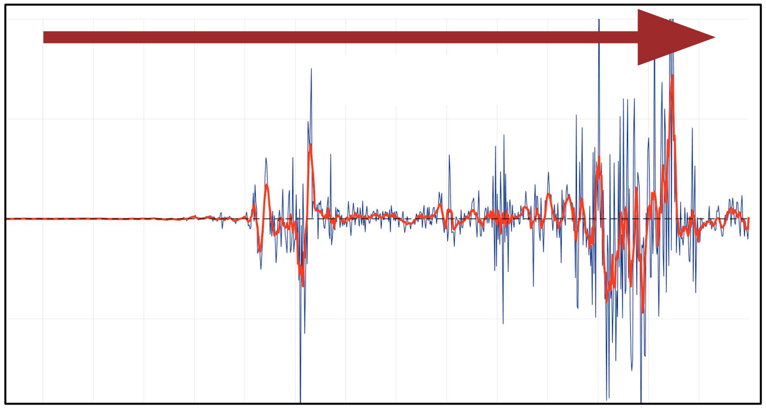

- ✔ Characteristics
- ✔ Dependence on IMF clock angle
- ✔ Dependence on solar zenith angle

- ✘ Characteristics
- ✘ Dependence on IMF clock angle
- ✘ Dependence on solar zenith angle
- ✘ Relationship between scales

Disagreement between Swarm FACs at large-scales (>350 km scale size)

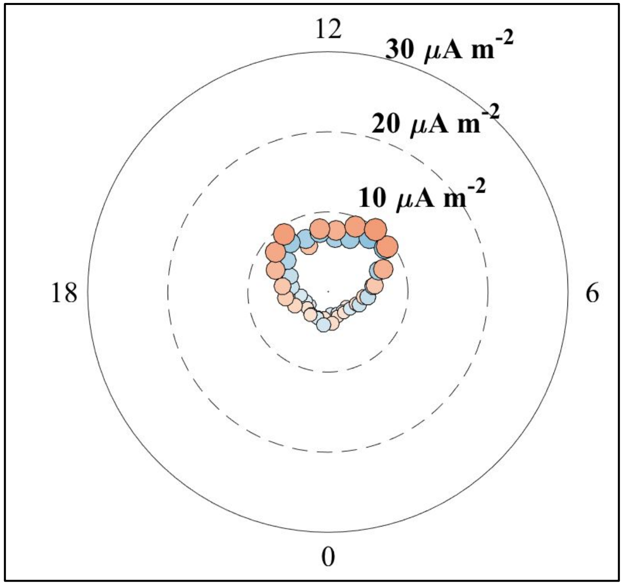

Disagreement between Swarm FACs at small-scales (~50 km scale size)

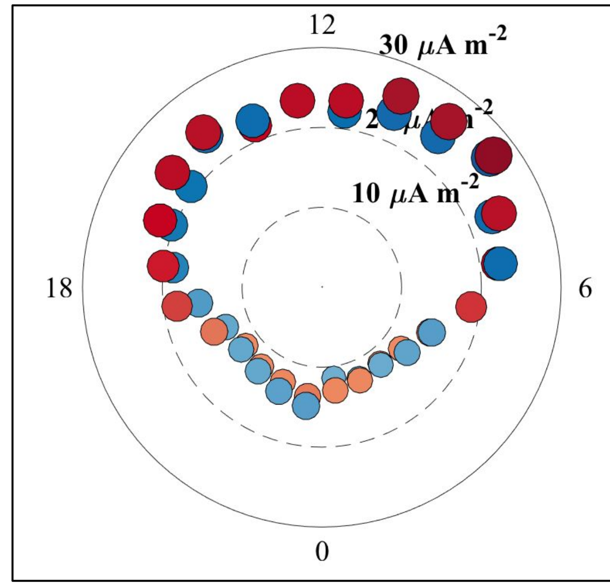

Away from ionosphere (upward FAC)
Toward ionosphere (downward FAC)
Size indicates magnitude

Radial direction: Increasing disagreement (difference between model and Swarm estimates)

1 Can this explain 'anomalous' magnetosphere-ionosphere-thermosphere behavior?

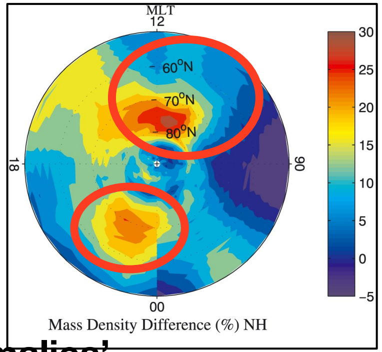

Neutral density 'anomalies'
[*Liu et al., 2005*]

Disagreement between Swarm FACs at small-scales (~50 km scale size)

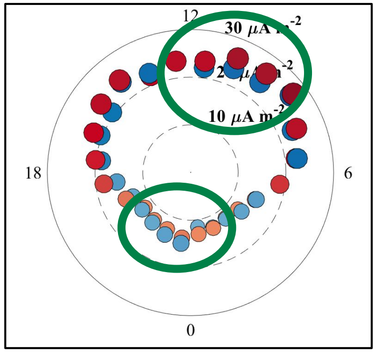

2 How do we examine the role of additional electrodynamic parameters and the impact on geospace?

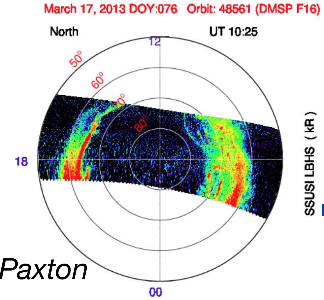

Courtesy: Larry Paxton

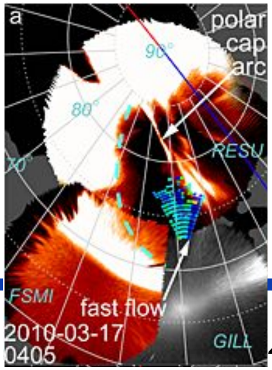

Zou et al., [2015]

Qingyu

Impacts of multi-scale FACs on the IT system: GITM study

[1]Qingyu Zhu, [1]Yue Deng, [2]Arthur Richmond, [3,4]Ryan McGranaghan, [2]Astrid Maute
[1]UTA; [2]HAO, NCAR; [3]UCAR; [4]JPL

2018 CEDAR, Santa Fe

Introduction & Motivation

- **FACs are critical for MIT coupling study**
  - Large-scale FAC pattern has been well established
  - Departures from the large-scale FAC pattern cannot be simply ignored, particularly for those related with meso- and small-scale FACs.

- **How do FACs on different scales impact the IT system?**

☆ **Relationship between ionospheric electrodynamics and FAC:**

- Does ionospheric electric field have similar scale dependence as FAC?

Data and Model

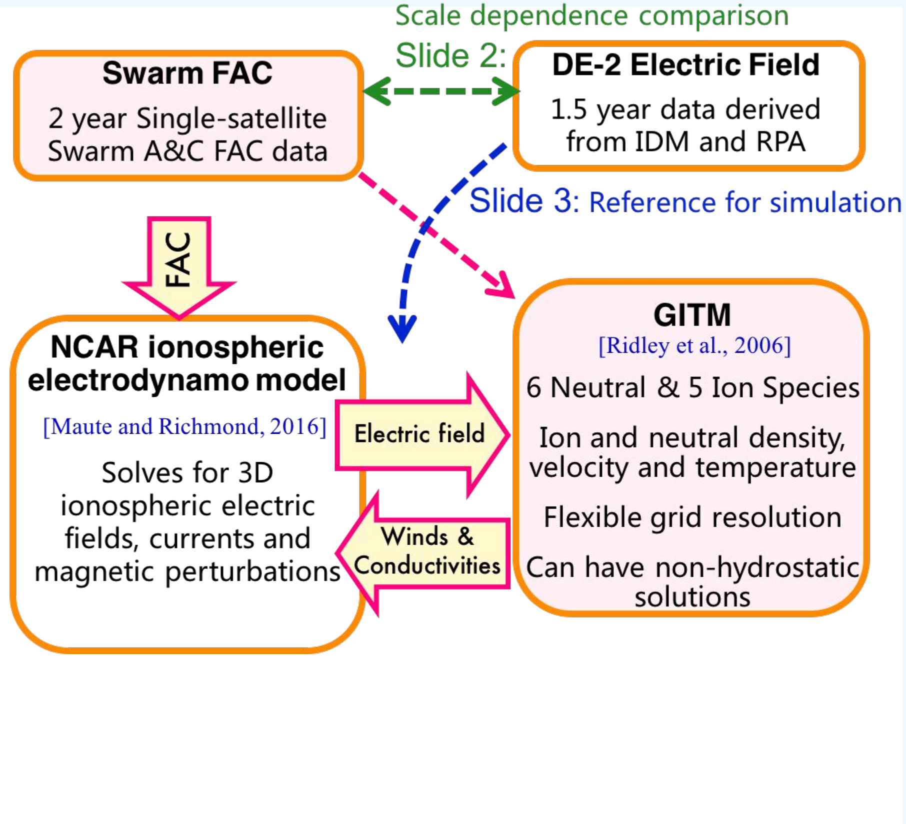

Swarm FAC

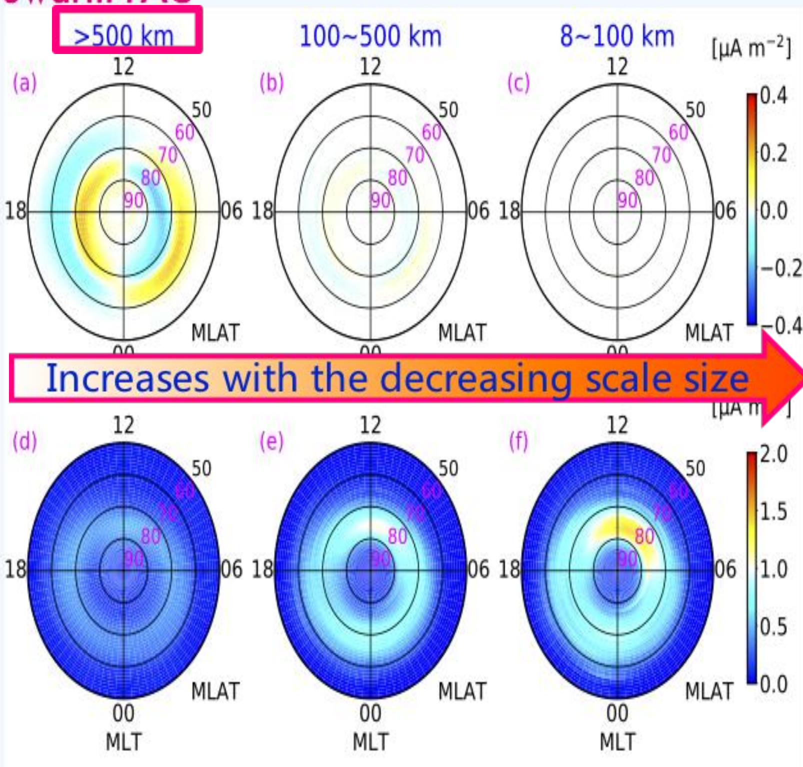

DE-2 electric field

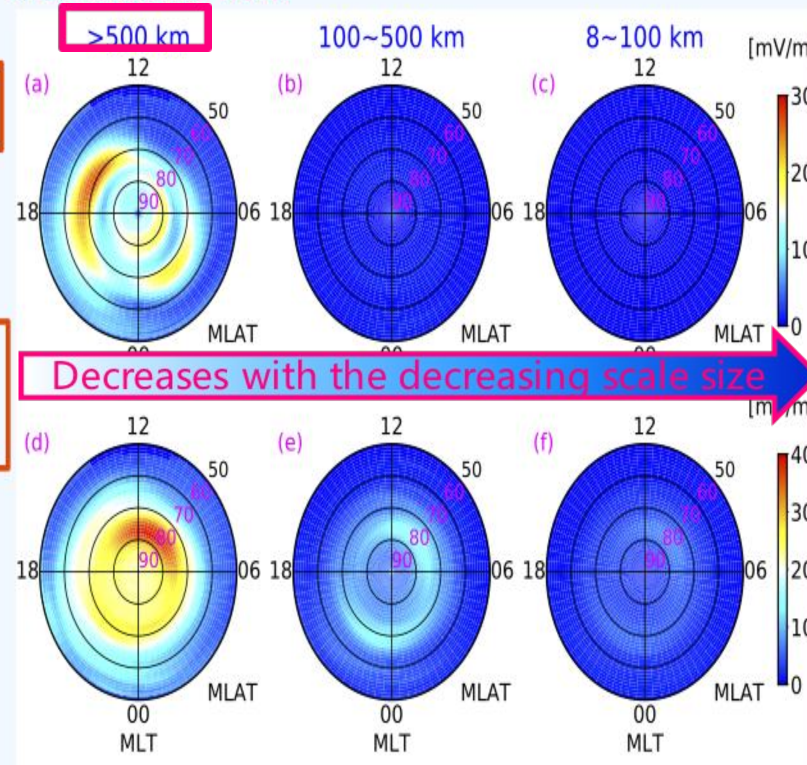

Average

Increases with the decreasing scale size

Standard deviation

Decreases with the decreasing scale size

Variability

Spectra of FAC and dBy

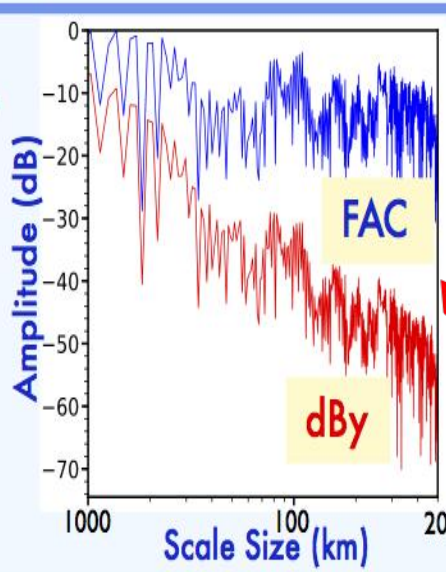

*dBy: E-W Magnetic perturbation

- Power spectra: dBy ≃ Ex (N-S electric field) [Weimer, 1985]
- dBy (Ex) ↘ as scale ↘
- FAC is roughly constant

Discrepancy between FAC ($J_\parallel$) and ionospheric electric field ($E_\perp$):

$J_\parallel = -\nabla_\perp \cdot (\boldsymbol{\Sigma} \cdot \mathbf{E}_\perp)$ → $J_\parallel = -\Sigma_P \dfrac{\partial E_x}{\partial x}$ → $|J_\parallel| \propto \dfrac{|E_x|}{L}$ → $|E_x| \propto |J_\parallel| L$

L: scale size

$|E_x|$↘ with L if constant $|J_\parallel|$

On meso-/small scale: Strong $J_\parallel$ ≠ Strong $\mathbf{E}_\perp$

Electric field variability

FAC-GITM **DE-2**

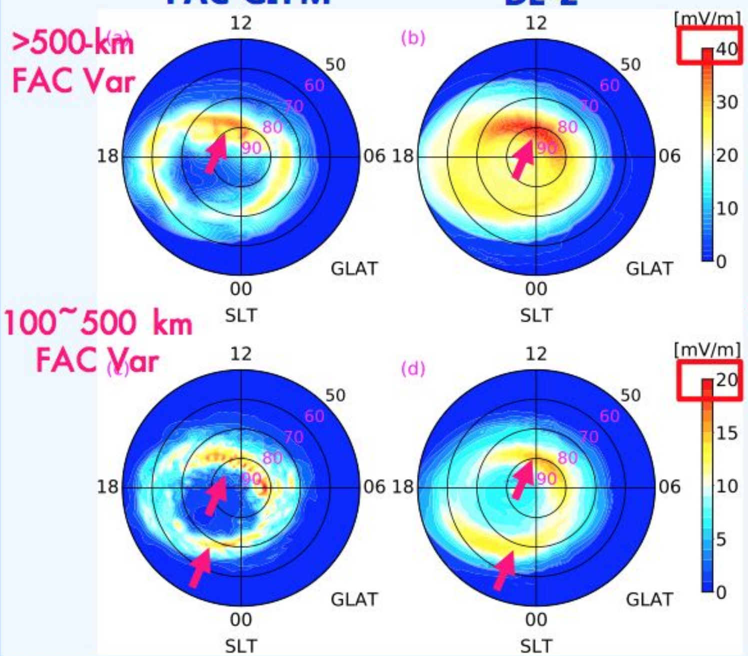

Simulation Results

Focus: Energy deposition

Key: FAC Var → E Var

An approach to include FAC variabilities

Joule heating enhancement

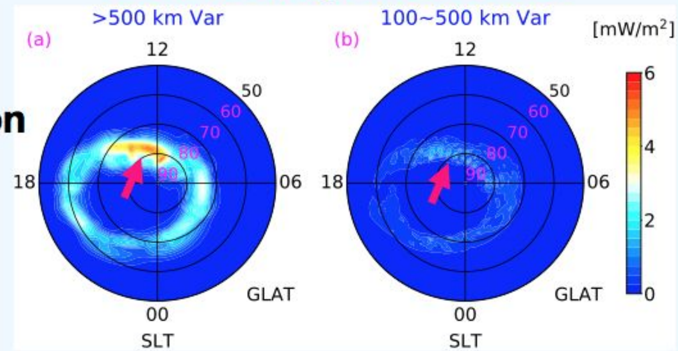

Comparing with no FAC Var case

Large-scale FAC Var	~5 mW/m^2 increase near the noon ~160% global enhancement
Mesoscale FAC Var	~1 mW/m^2 increase near the noon ~38% global enhancement

Summary

➜ $J_{\parallel}$ and $\mathbf{E}_{\perp}$ on mesoscale & small scale:

- $J_{\parallel}$ ↗ as scale ↘, $\mathbf{E}_{\perp}$ ↘ as scale ↘;
- **Strong $J_{\parallel}$ ≠ Strong $\mathbf{E}_{\perp}$.**

➜ High-latitude variabilities on energy deposition:

- Joule heating enhancement related to mesoscale variabilities is non-negligible.

Impacts of electric field & particle precipitation on mesoscale and small scale to Joule heating

1) Poster: **MITC-25**, WED, 4pm

2) Oral in "**High-latitude TI coupling**" session on THU, 1:30 pm

Thank you!

Kristina

data fusion: in situ plus imagery

High lat challenges :

"mesoscale structuring at high latitudes"

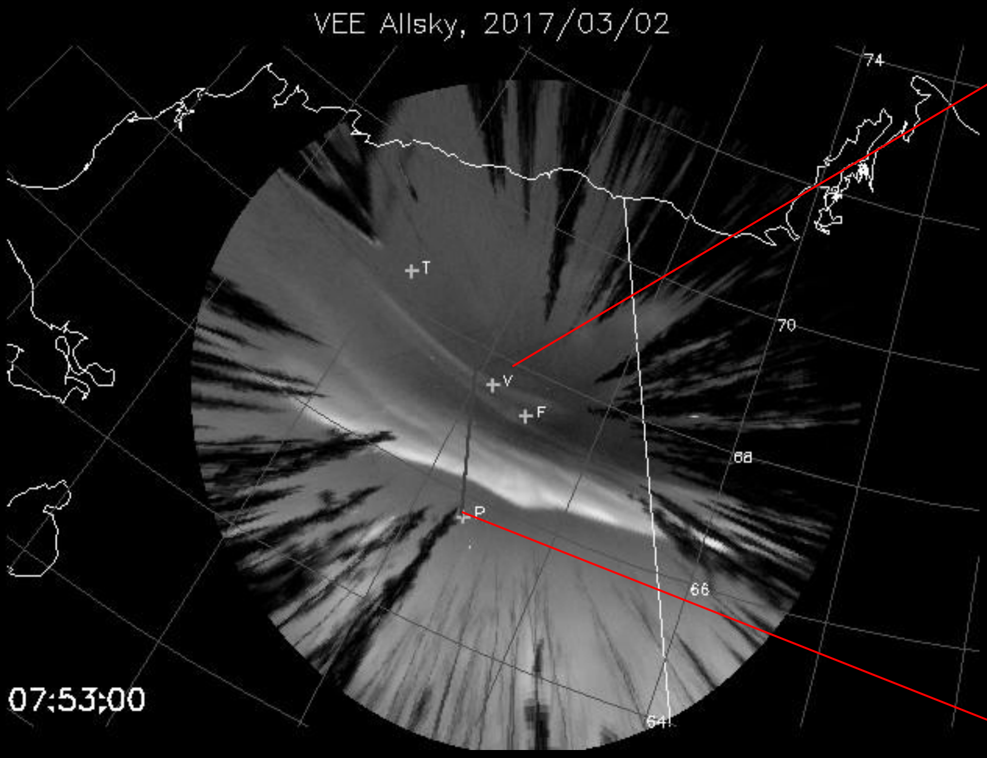

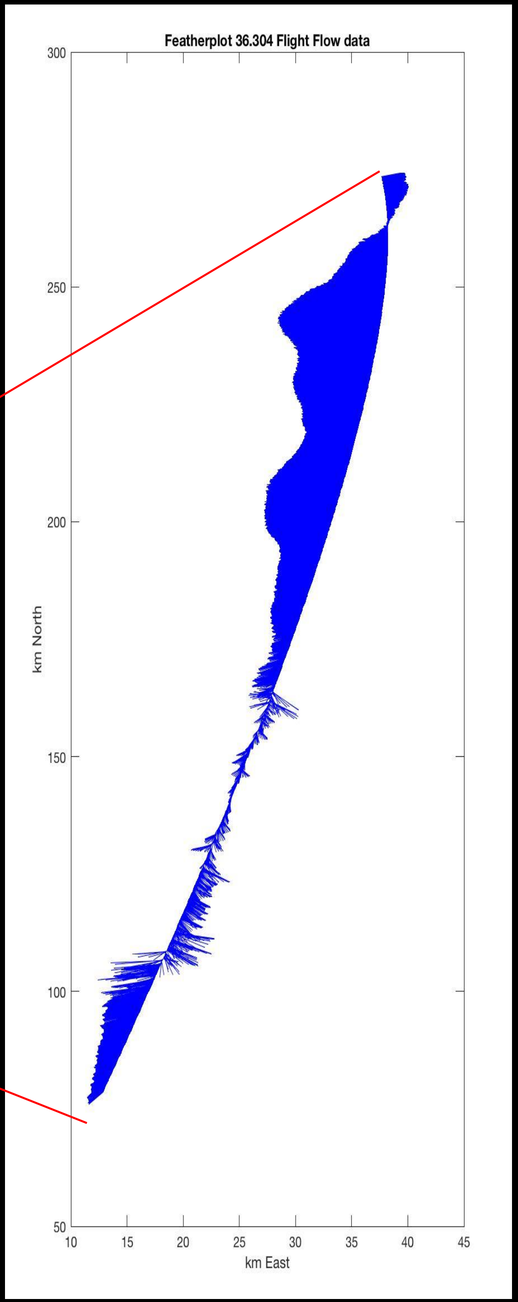

K Lynch

Dartmouth Physics

Ref, Isinglass team

Cedar Meeting, HiLat Challenges, June 2018, Santa Fe

Ionospheric current continuity rules

$\int E_{Hi} \cdot dl = -\Phi_{arc} = \mathcal{E}_{char}$

$\nabla \cdot J = 0 = \nabla_{||} \cdot J_{||} + \nabla_{\perp} \cdot J_{\perp}$

At ionospheric footpoint,

$\nabla_{||} \cdot J_{||} = J_{||} = -\nabla_{\perp} \cdot J_{\perp} = \nabla_{\perp} \cdot (\Sigma \cdot E_{\perp})$

so

$$J_{||} \;=\; \Sigma_p(\nabla_{\perp} \cdot \mathbf{E}_{\perp}) + \nabla_{\perp}\Sigma_p \cdot \mathbf{E}_{\perp} - \nabla_{\perp}\Sigma_h \cdot (\hat{\mathbf{e}}_1 \times \mathbf{E}_{\perp})$$

Now, also

$J_{||} = \mathcal{E}_{flux} / \mathcal{E}_{char}$

so

$\mathcal{E}_{flux} = \mathcal{E}_{char} \cdot J_{||}$

and brightness gradient is

$\nabla \mathcal{E}_{flux} = \mathcal{E}_{char} \cdot \nabla J_{||} + \nabla \mathcal{E}_{char} \cdot J_{||}$

The last term gives back the high-altitude $\mathbf{E_{Hi}}$, and the other term involves conductivity gradients and ionospheric electric field divergences.

Ref, i.e., Brekke et al., 1997

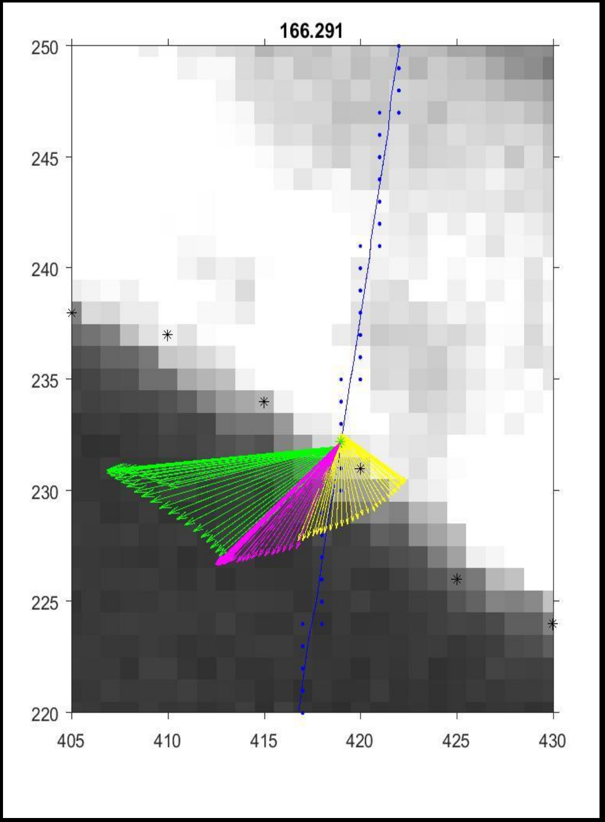

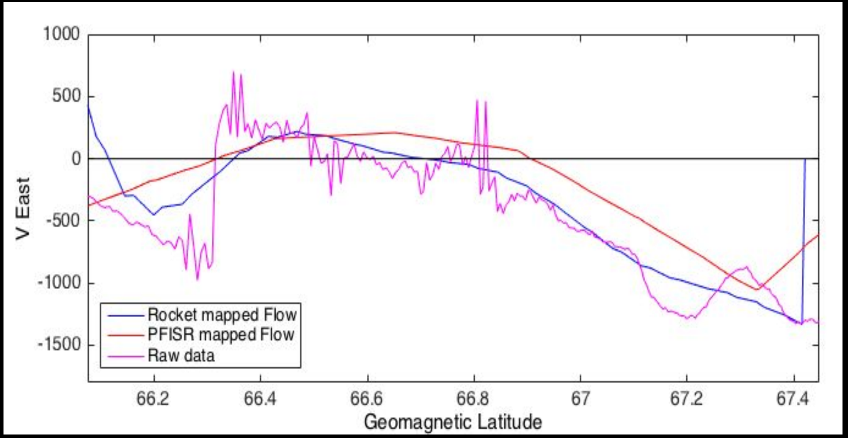

R Clayton, 2018

Mission Concept

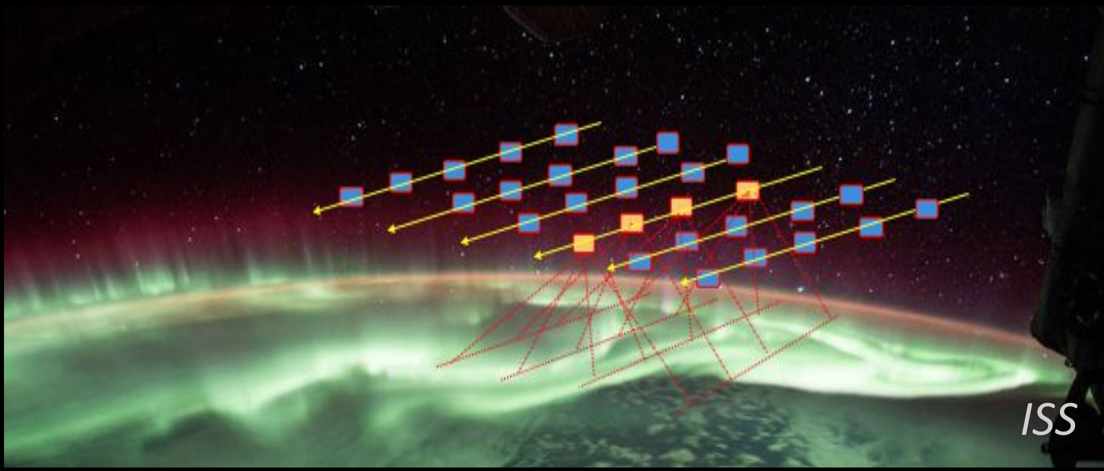

- What is the role of the ionosphere in the creation of auroral arcs?

ARCS
AURORAL RECONSTRUCTION CUBESWARM

Phase Four

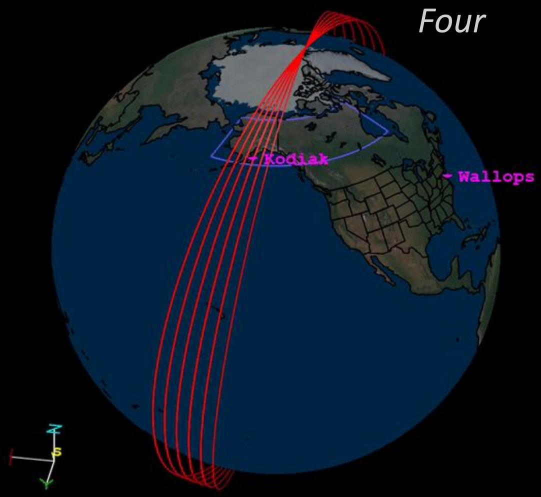

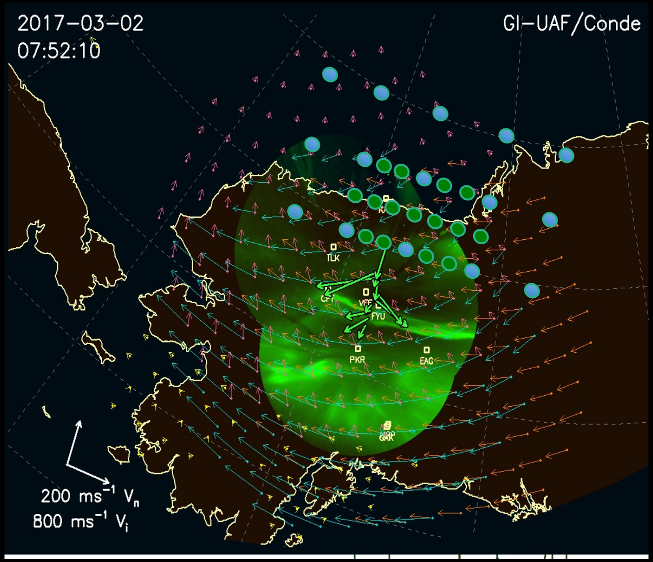

Bea

PCB identification using Redline ASIs

Bea Gallardo-Lacourt, Emma Spanswick, Megan Gillies, Elizabeth Roy, Eric Donovan, Aaron Ridley, and Dongjie Gou

- Blanchard et al. [1997] used MSP redline emission +DMSP-9 to located the optical PCB
- **Here we used DMSP as a benchmark for identifying the PCB in REGO**
- 6300Å emission is sensitive to low energy precipitation. It has an extended altitudinal distribution [150km-400km]

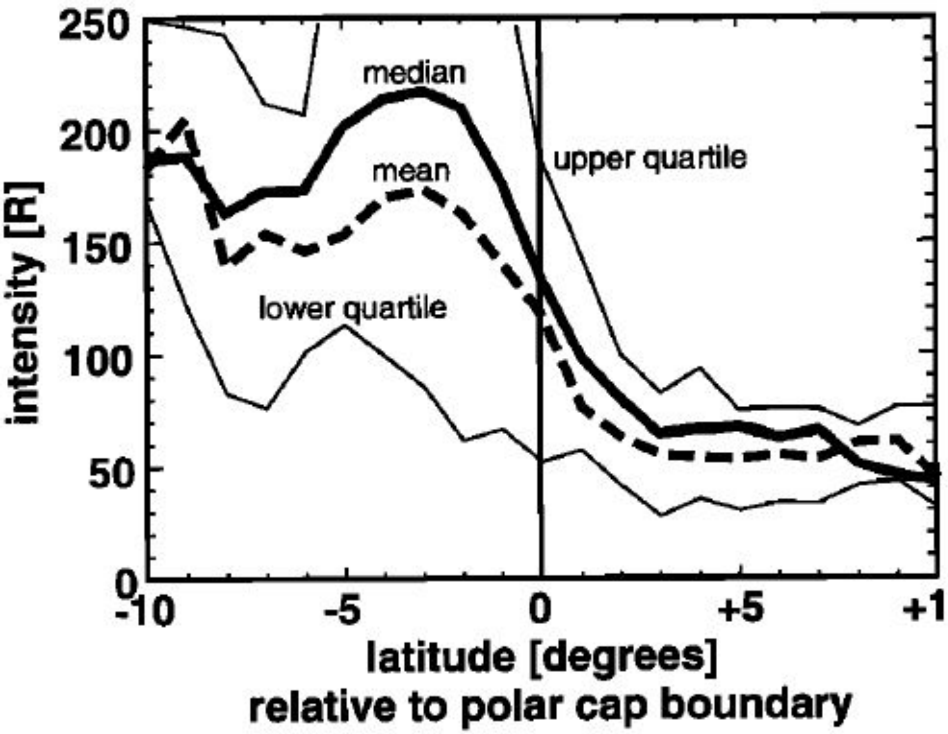

[Blanchard et al., 1997]

PCB identification using Redline ASIs

<u>Bea Gallardo-Lacourt</u>, Emma Spanswick, Megan Gillies, Elizabeth Roy, Eric Donovan, Aaron Ridley, and Dongjie Gou

- Blanchard et al. [1997] used MSP redline emission +DMSP-9 to located the optical PCB
- **Here we used DMSP as a benchmark for identifying the PCB in REGO**
- 6300Å emission is sensitive to low energy precipitation. It has an extended altitudinal distribution [150km-400km]

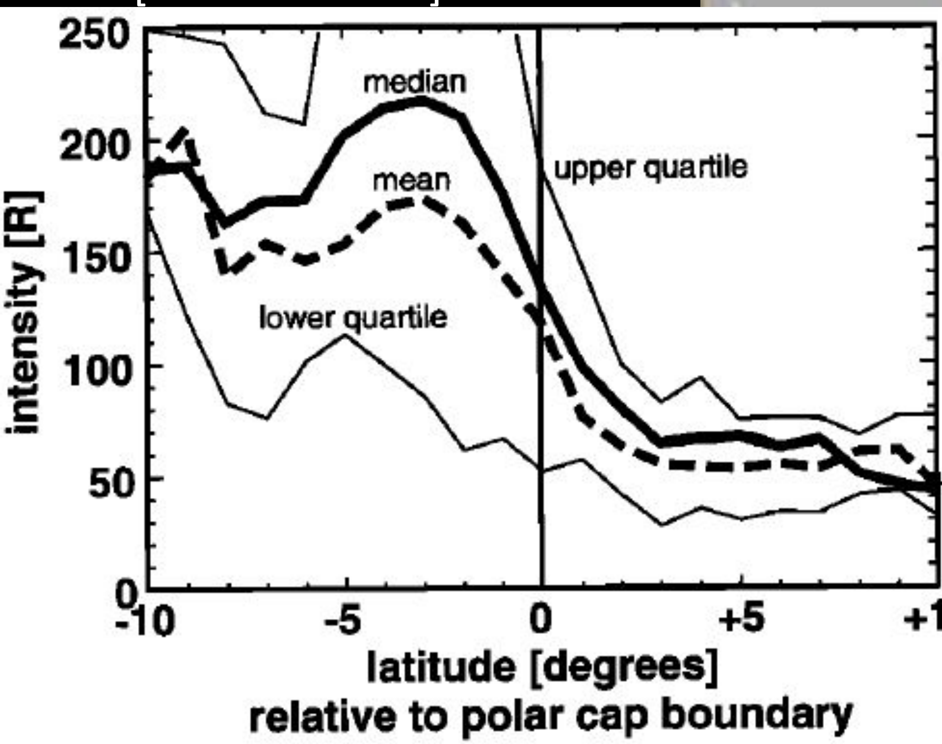

[Blanchard et al., 1997]

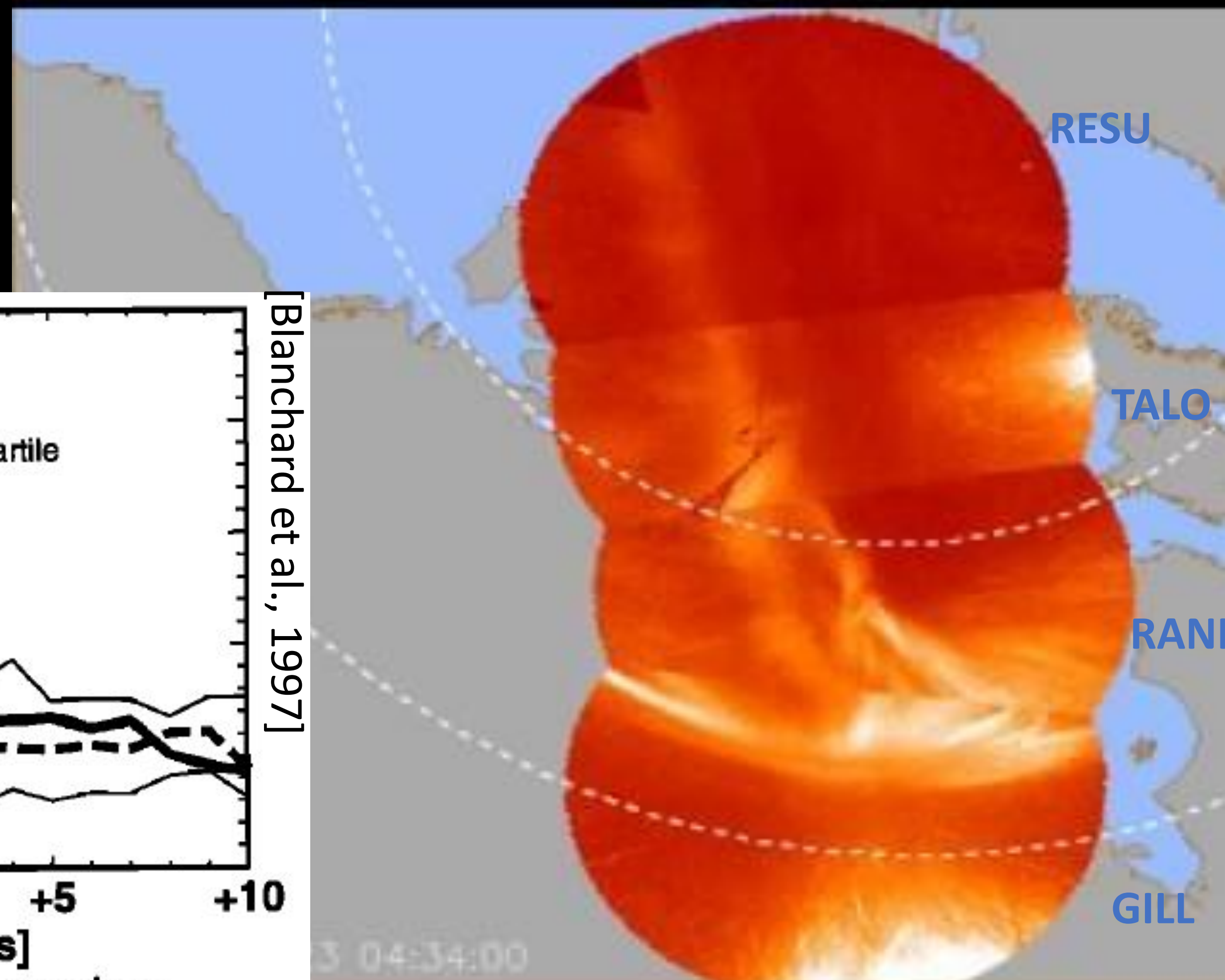

REGO + DMSP conjunctions

- REGO: Red Line Geospace Observatory. Active since November 2014 up to date
  9 ASIs covering North America sector working in 3s time resolution
- DMSP-16: Defense Meteorological Satellite Program. Active since 2003
- We analyzed 50 events using REGO Rankin Inlet (RANK) ASI and DMSP-16. From November 2014 to March 2016
- We plan to extend this study to more ASIs and DMSPs to improve our statistic

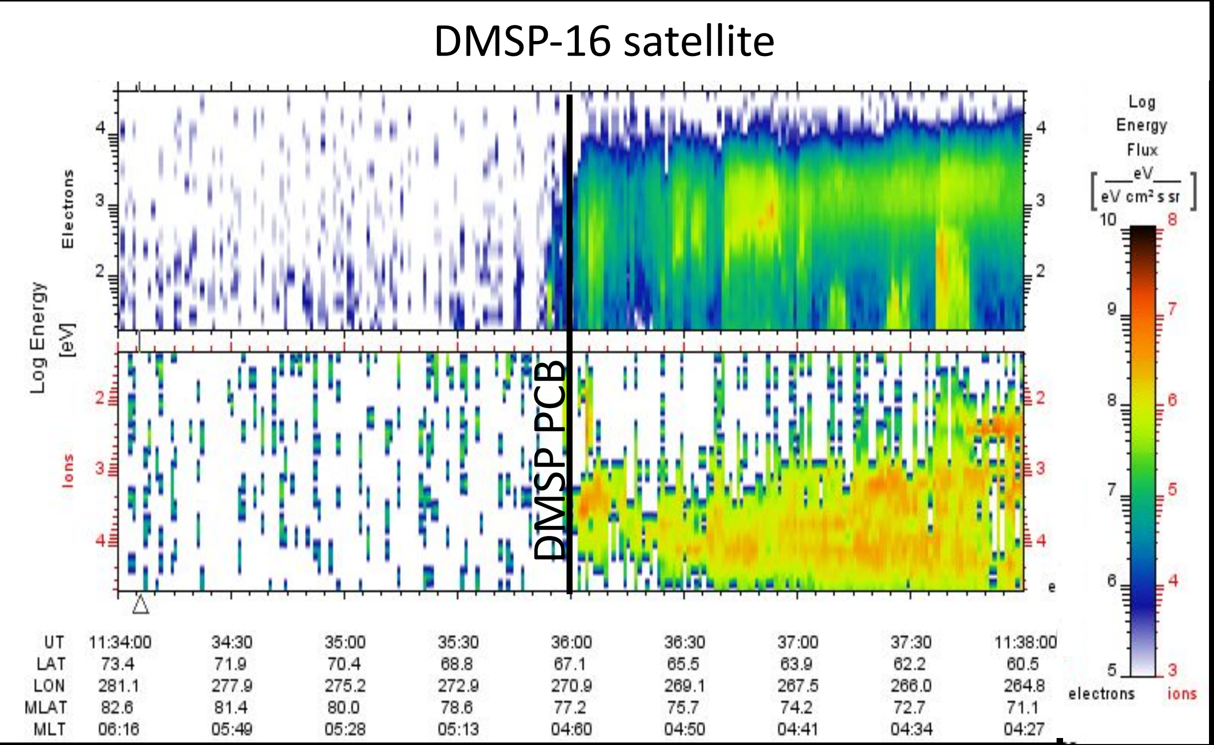

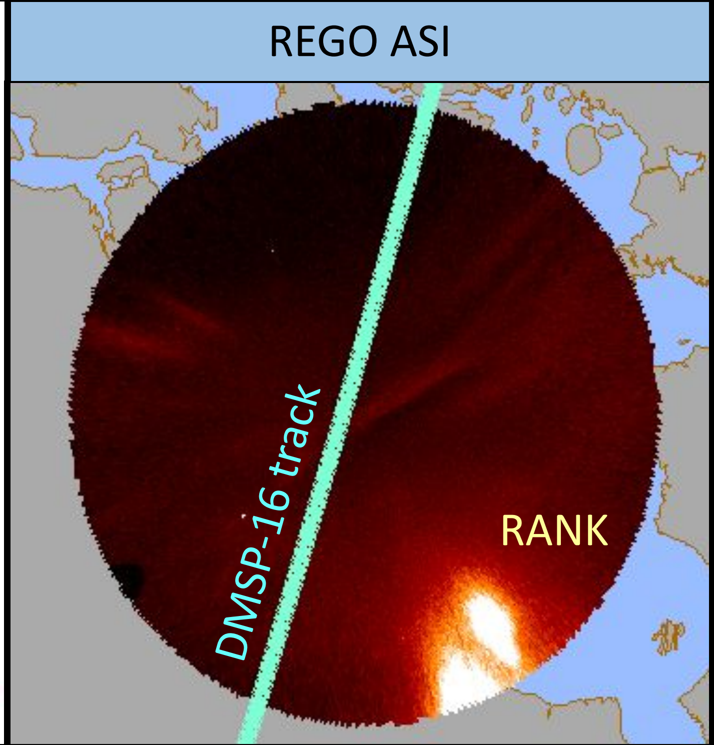

REGO + DMSP conjunctions – Different mapping altitudes

- Max. luminosity ~4˚ equatorward than DMSP-PCB
- Luminosity decreased ~80% at the location of satellite boundary

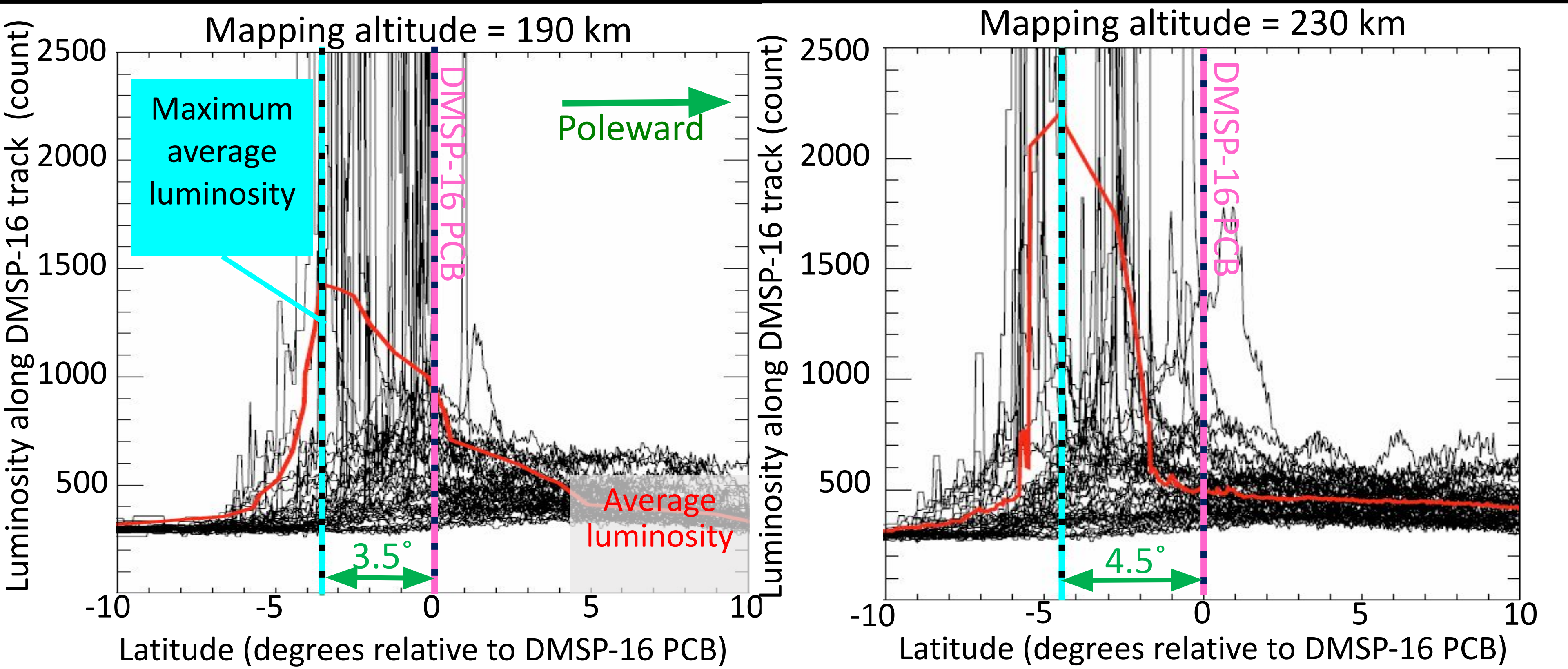

- Gillies et al., [2017] estimated the minimum altitude for the 6300Å emission to be at 190km
- Discontinuities observed in arcs if redline is mapped to lower altitudes

CONCLUSION

- On average, max. luminosity located ~4˚ equatorward of PCB , consistent w/Blanchard et al. 1997

Andy

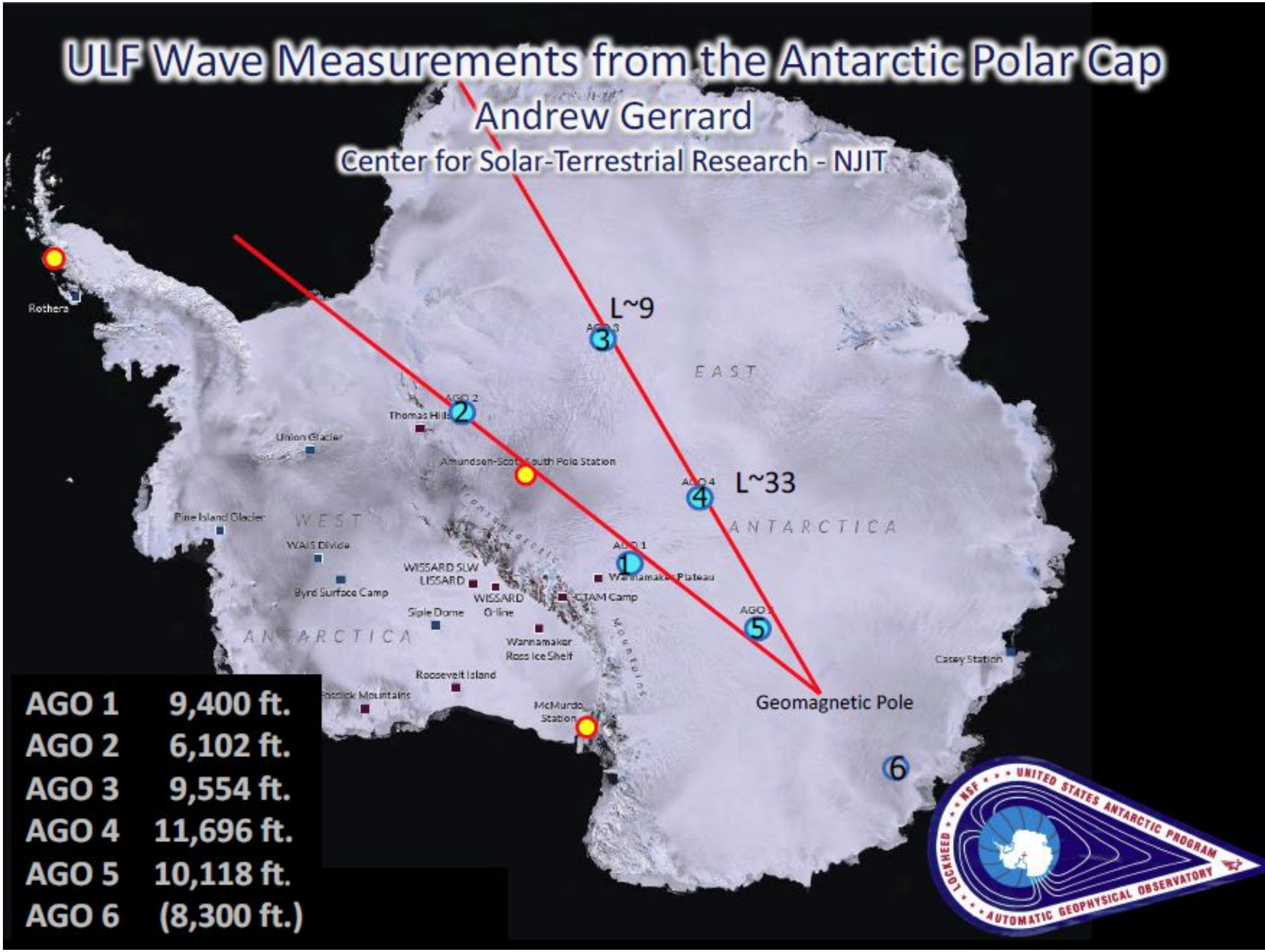

Andrew Gerrard, NJIT

Solar Wind ULF Coupling Into the Polar Cap

AGO5 March Climatology

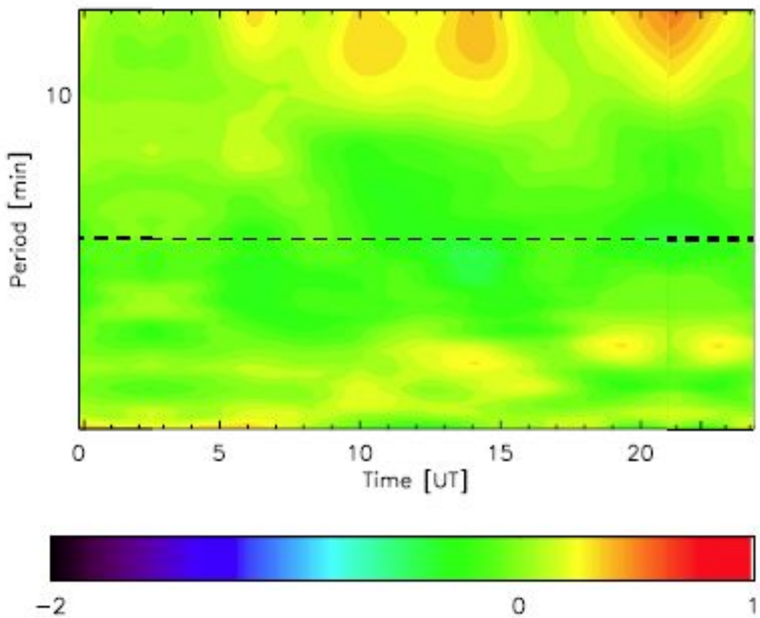

AGO5 March Synoptics

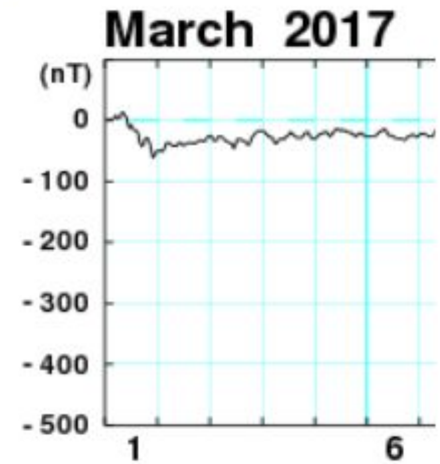

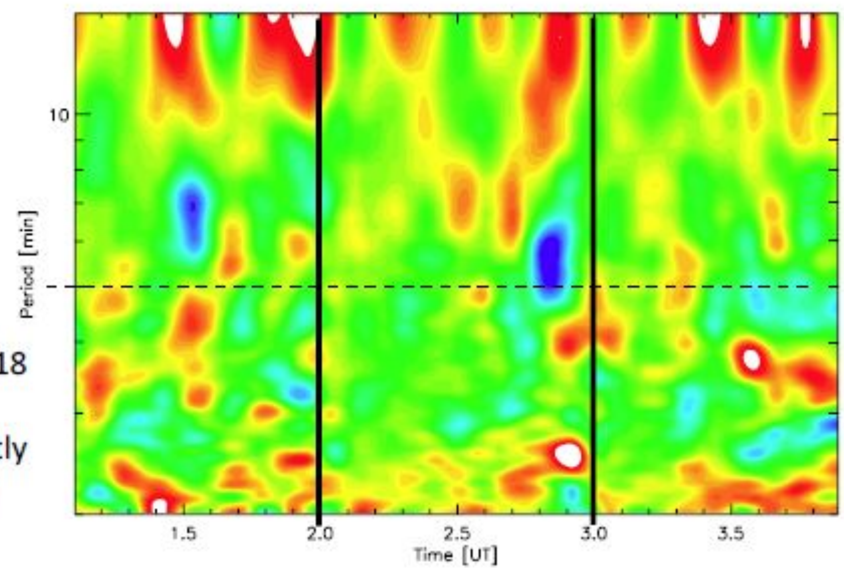

- Climatologies demonstrated in Frissell et al., 2018 GEM-CEDAR poster
- ULF features seen on March 1 at AGO5 are directly related to solar wind ULFs (e.g., Urban et al. [2016])

"Direct solar wind ULF influence"

Magnetospheric ULF Coupling Into the Polar Cap

AGO3 March Climatology

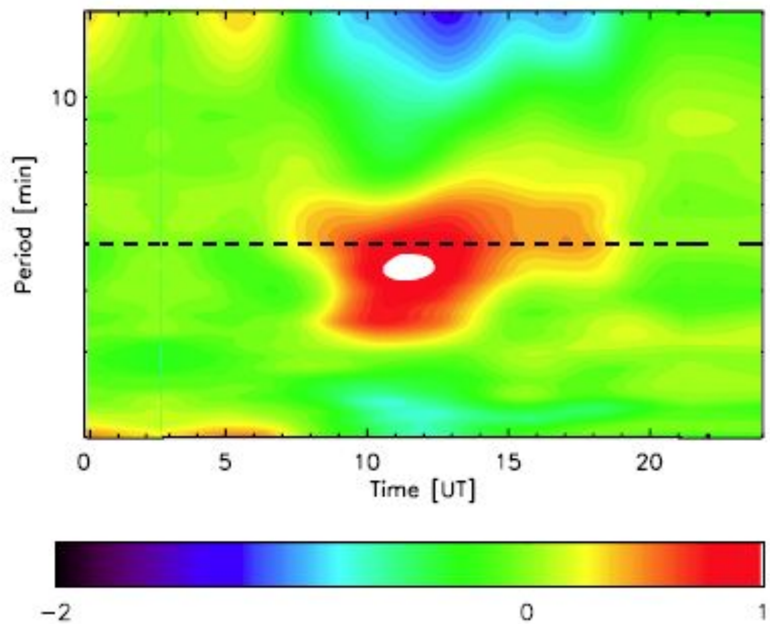

AGO3 (L~9) March Synoptics

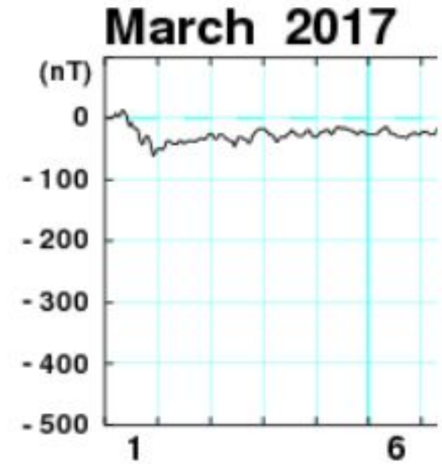

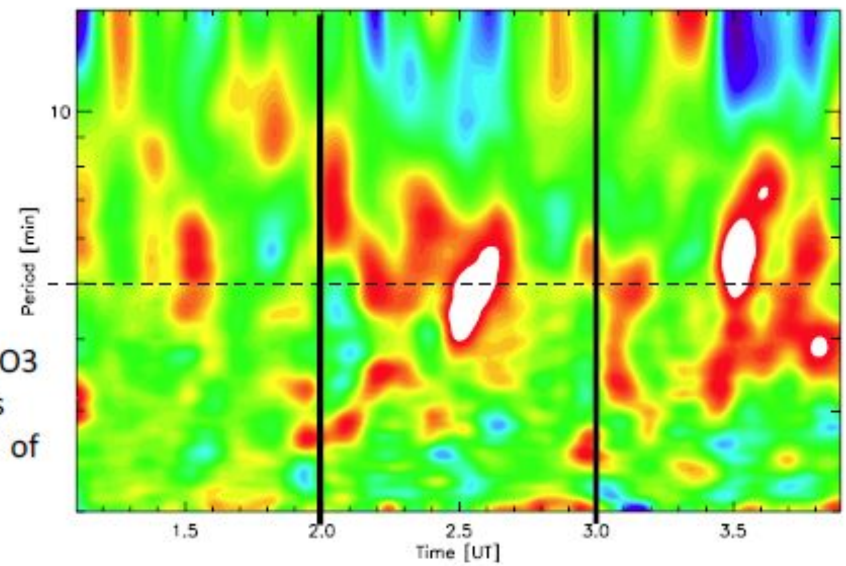

- ULF features seen on nightside March 1-2 at AGO3 (and AGO2), which are not related to solar wind ULFs
- In dusk-midnight sector, RBSPICE (L~6) sees lots of injections.
- ULFs associated with injections? ***RIP!***

- Drift-mirror mode? e.g., Cohen et al. [2016], Cooper et al. GEM2018 Poster, Soto-Chavez et al. [2018]

"In-direct solar wind ULF influence"

Craig

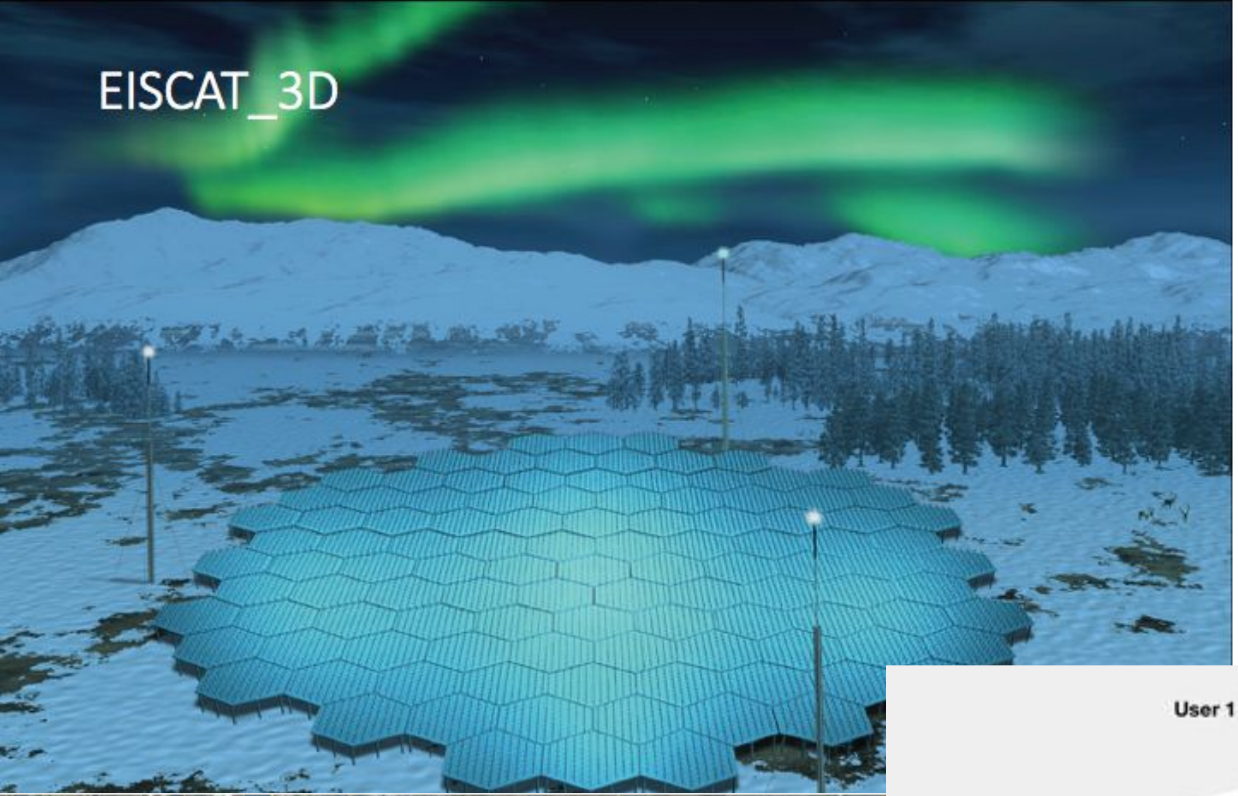

Craig Heinselman
EISCAT Scientific Association

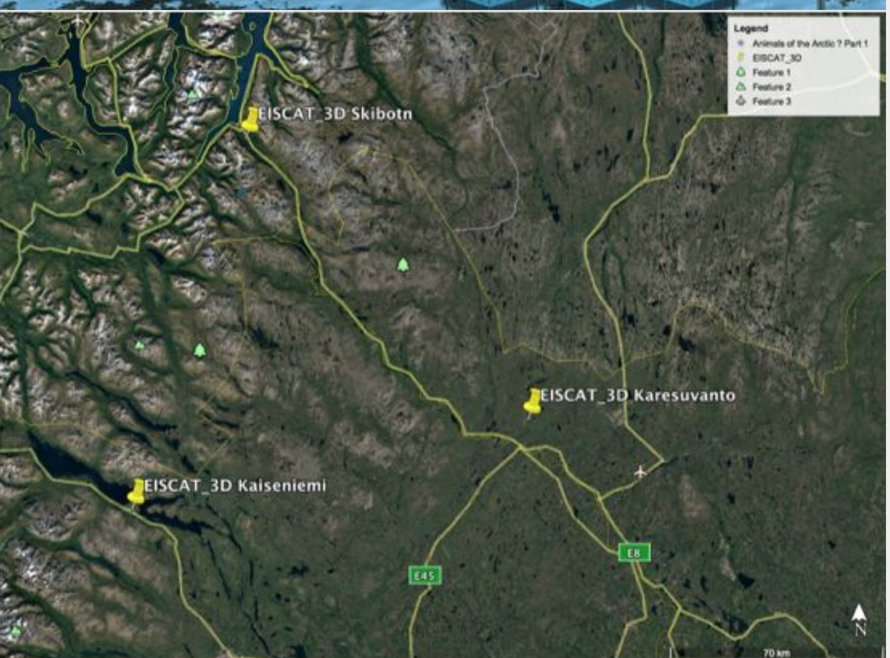

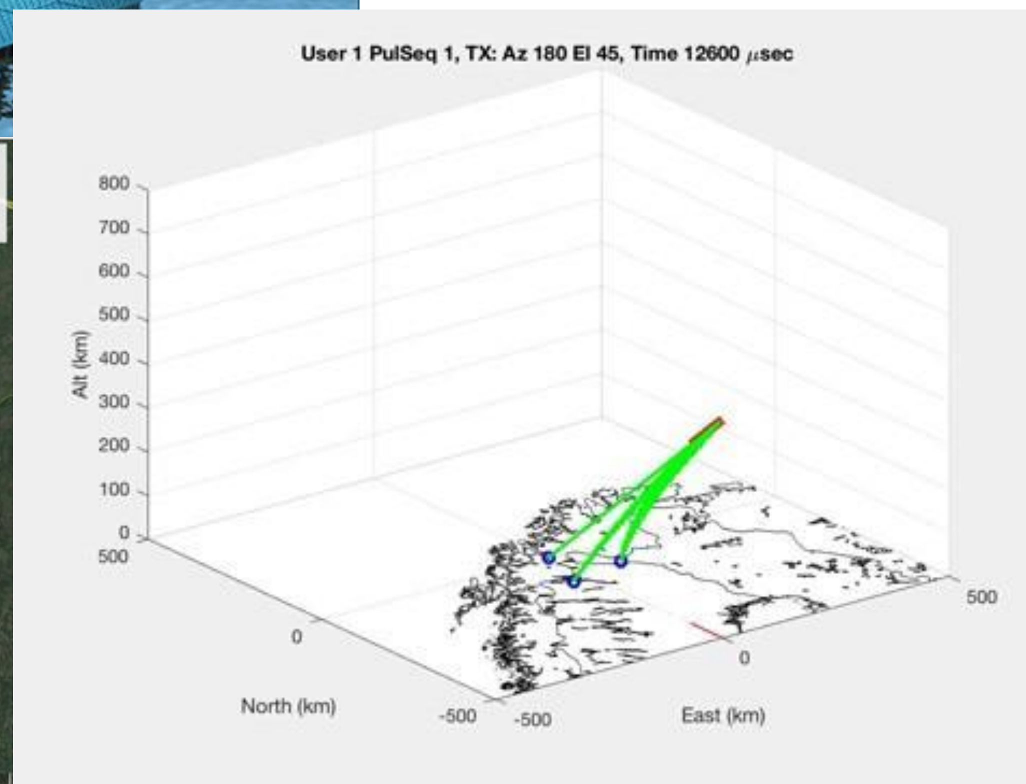

Kinds of measurements - Auroral Structure

Power profile: 0.44 sec, 0.9 km range

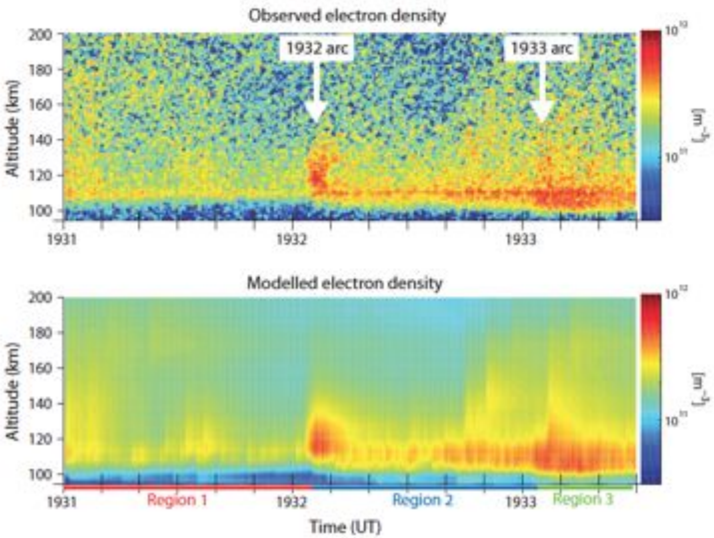

Fig. 7. Top: E-region enhancements in electron density corresponding to auroral arcs drifting over EISCAT. Bottom: modelled electron density.

Dahlgren et al., 2011

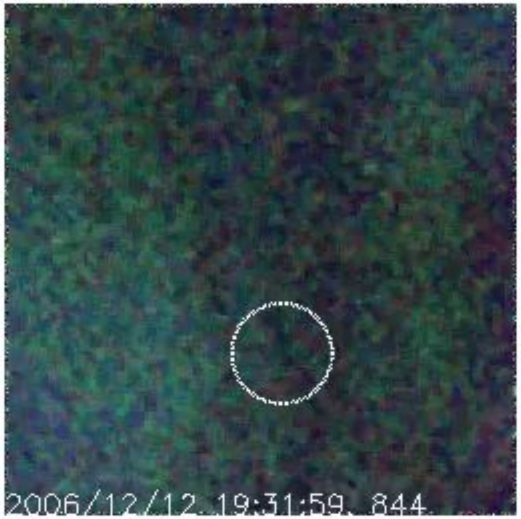

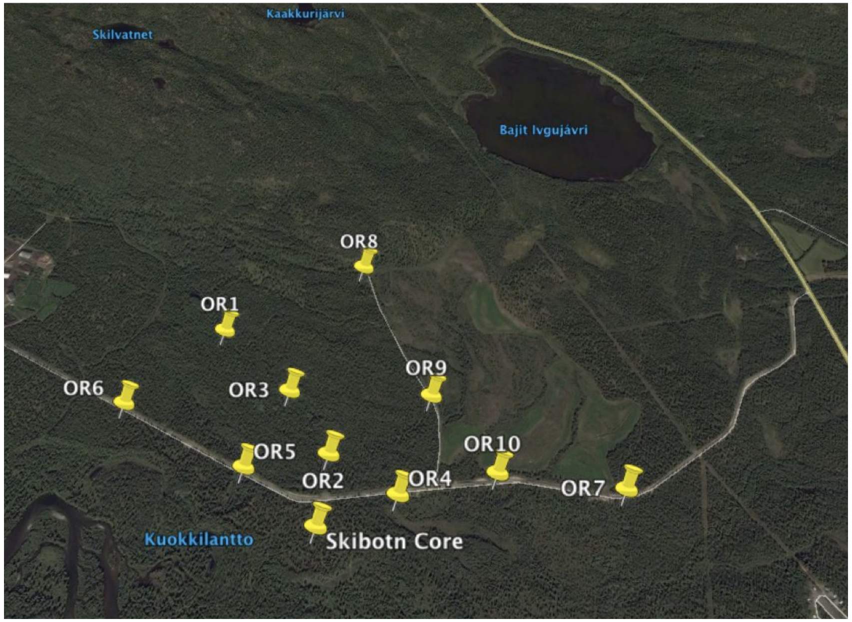

EISCAT Scientific Association

Speed Maps

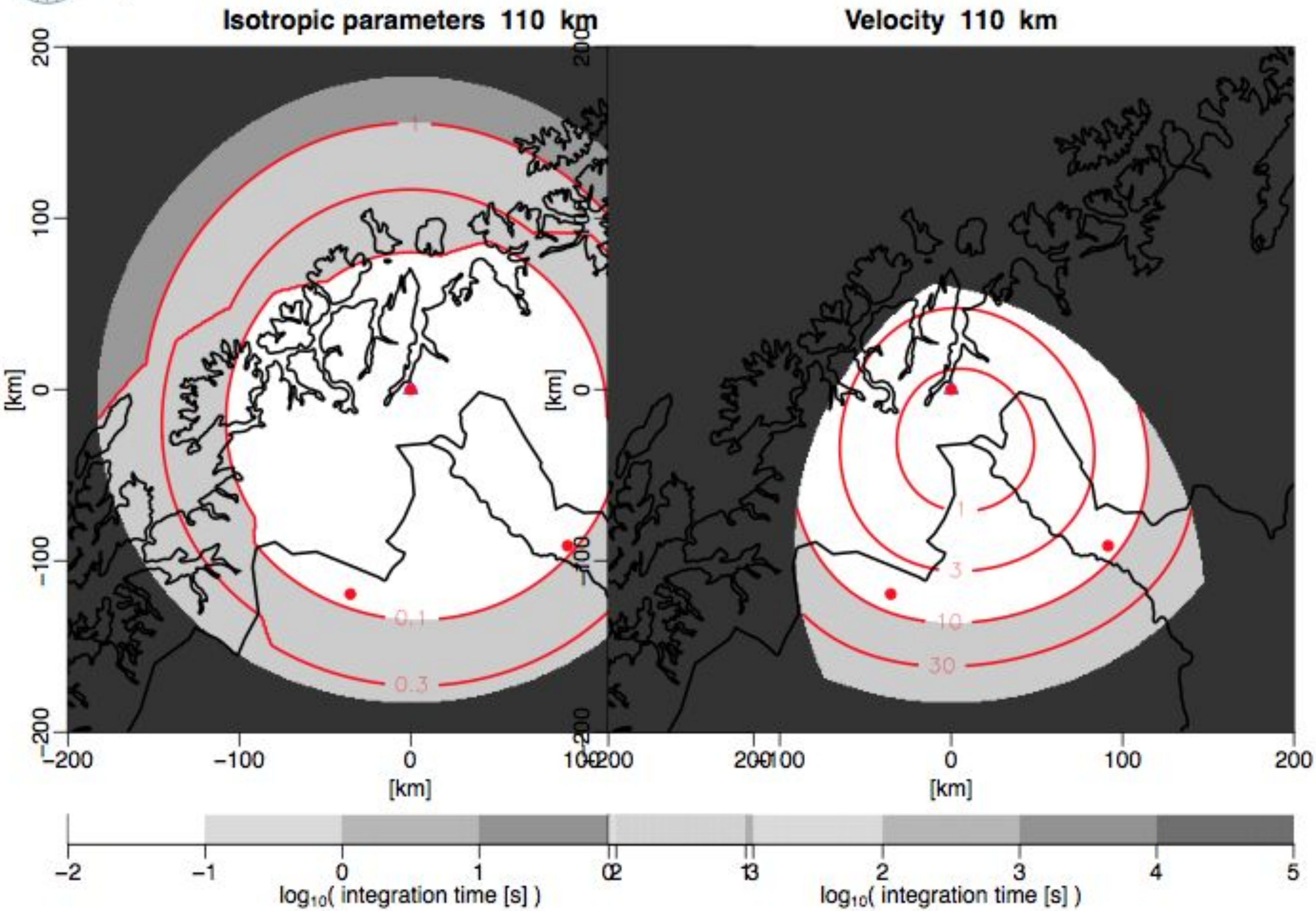

Evan

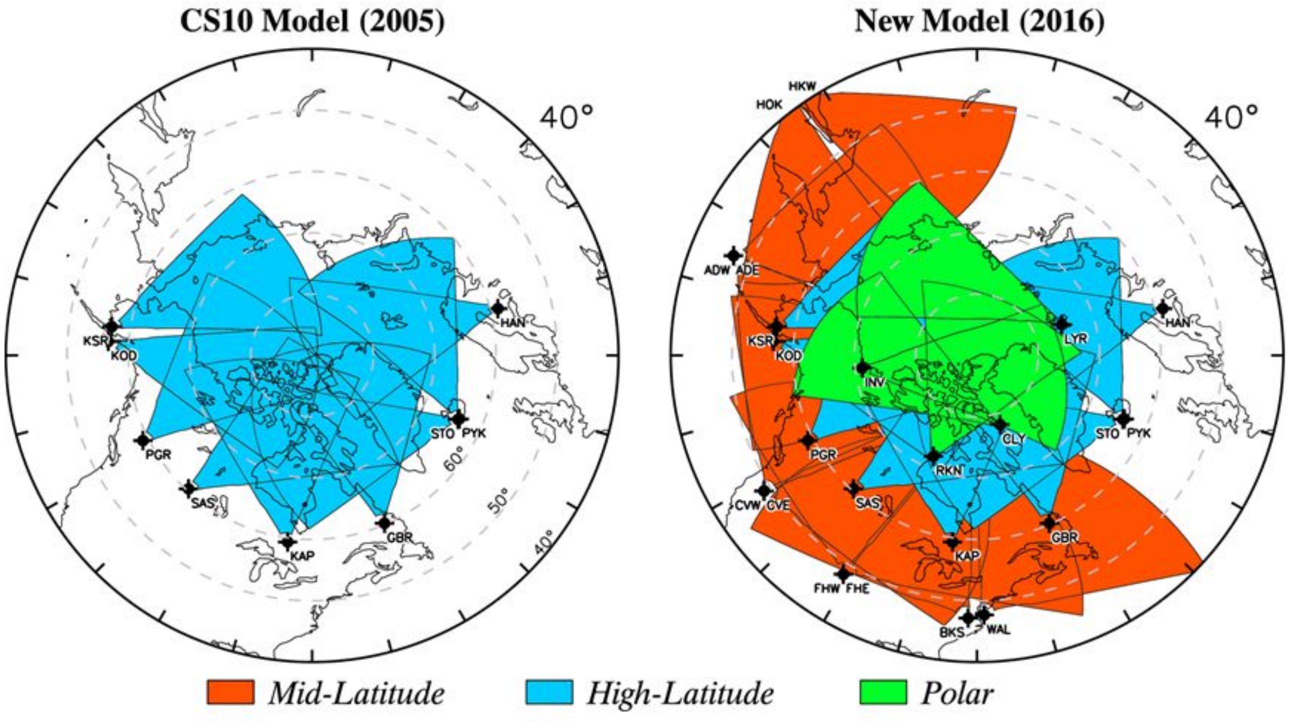

- We have recently derived an empirical model of ionospheric convection including mid-latitude and polar SuperDARN HF radar velocity measurements for the first time [*Thomas and Shepherd*, 2018]

TS18 Convection Model

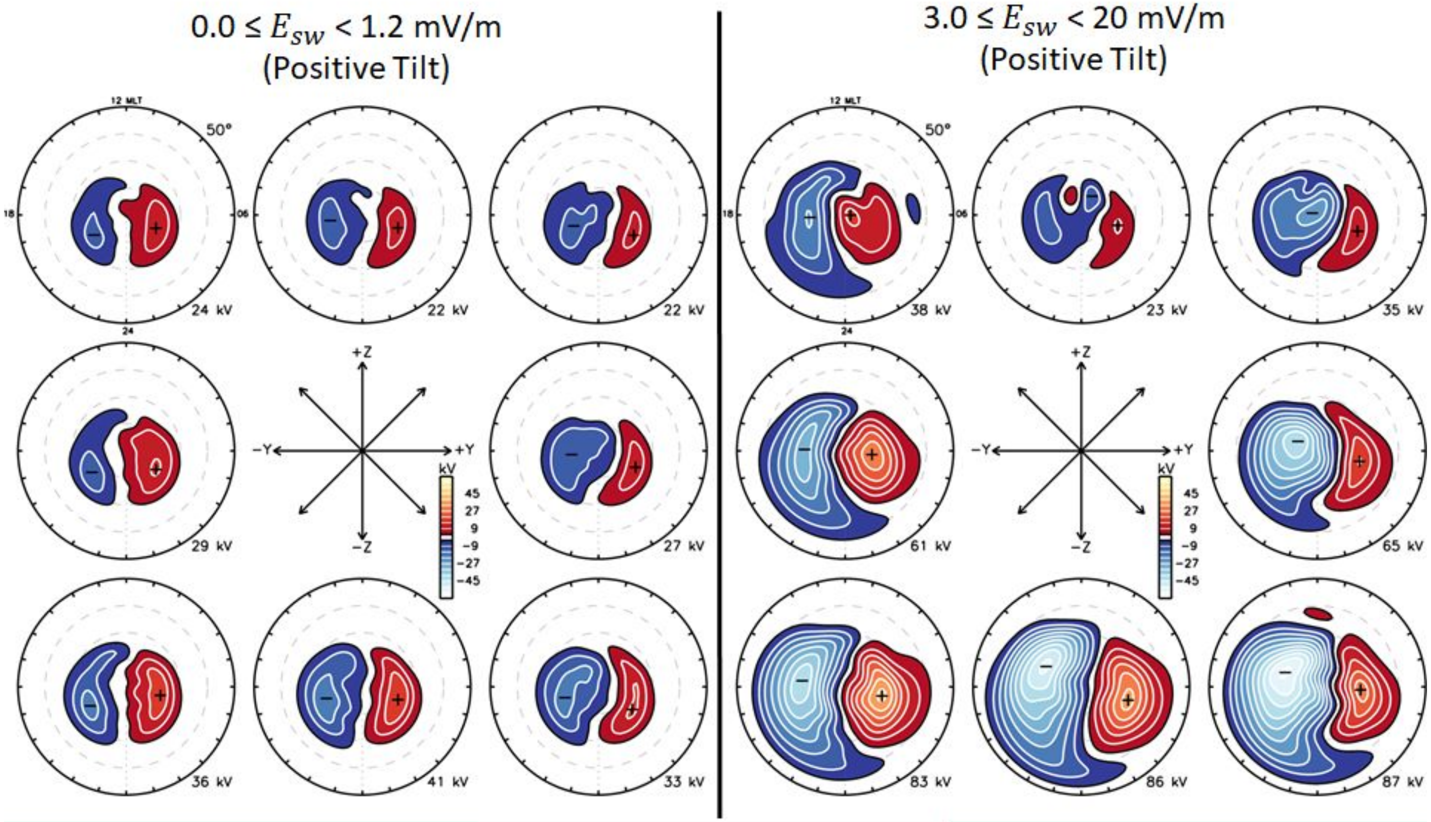

- Inclusion of mid-latitude radar data can increase the total measured cross-polar cap potential drop by as much as 40%

- Polar radars provide a smaller contribution to the total cross-polar cap potential drop, but provide an improved specification of plasma flows in the deep polar cap

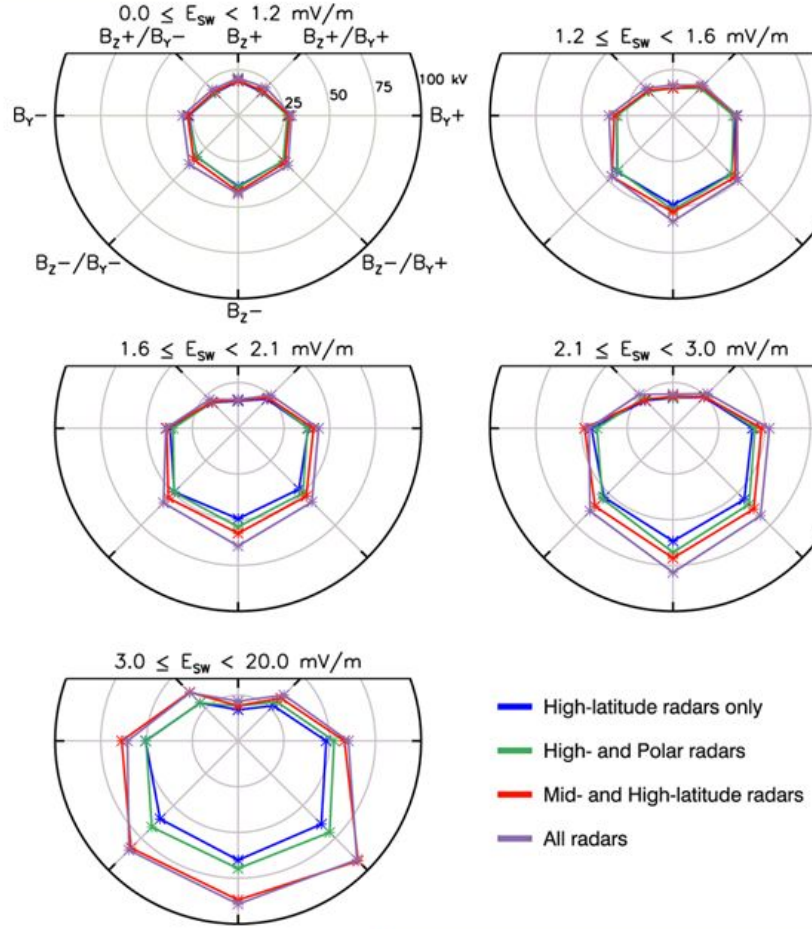

Rob G.

Effect of polar cap patches on SuperDARN measurements

R. G. Gillies[1], G. W. Perry[1], R. Varney[2], D. M. Gillies[1], and E. Donovan[1]
University of Calgary[1], SRI International[2]

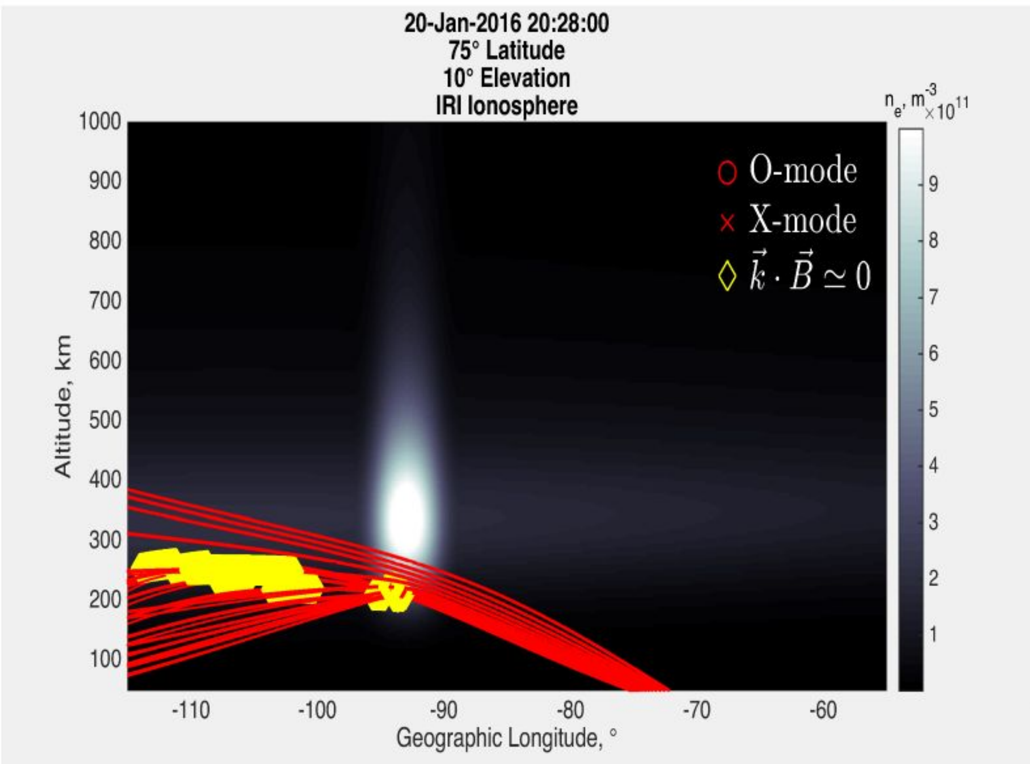

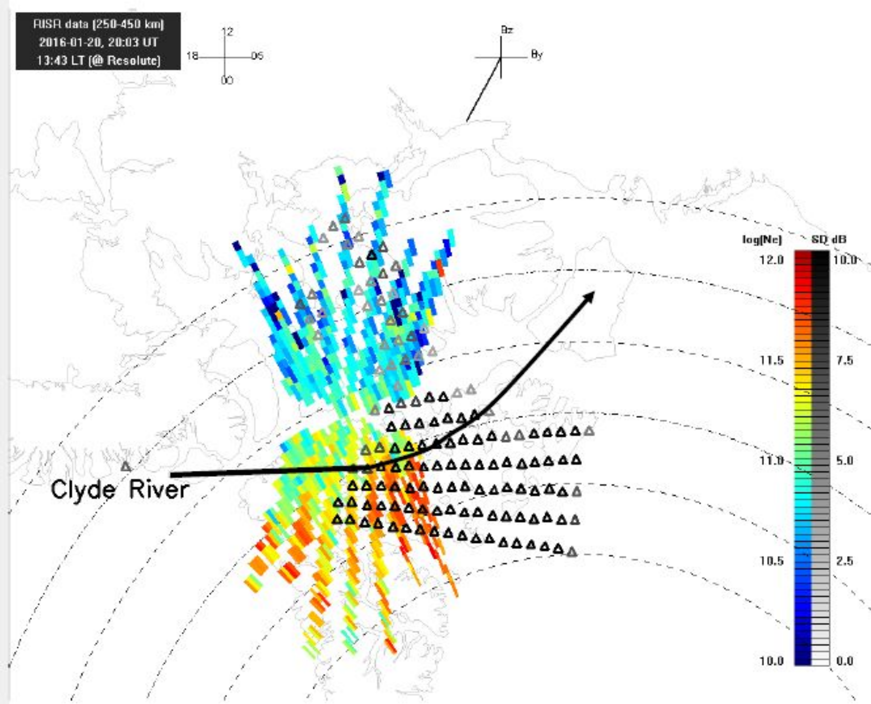

- HF propagation and resulting coherent scattering behavior is greatly affected by refraction from high density gradients

SuperDARN scatter around polar patch

- Polar patch observed by RISR-C and RISR-N on 2016-01-20
- Scatter from Rankin Inlet (diamonds) and Clyde River (triangles) SuperDARN radars received within and around the patch
- Scatter always on far edge of patch from respective radar
- This behavior occurs when there is one isolated patch:
    - Multiple patches passing through SuperDARN FOVs complicates the situation
- Conclusion: detection/localization of irregularities using SuperDARN HF scatter is complicated by propagation conditions

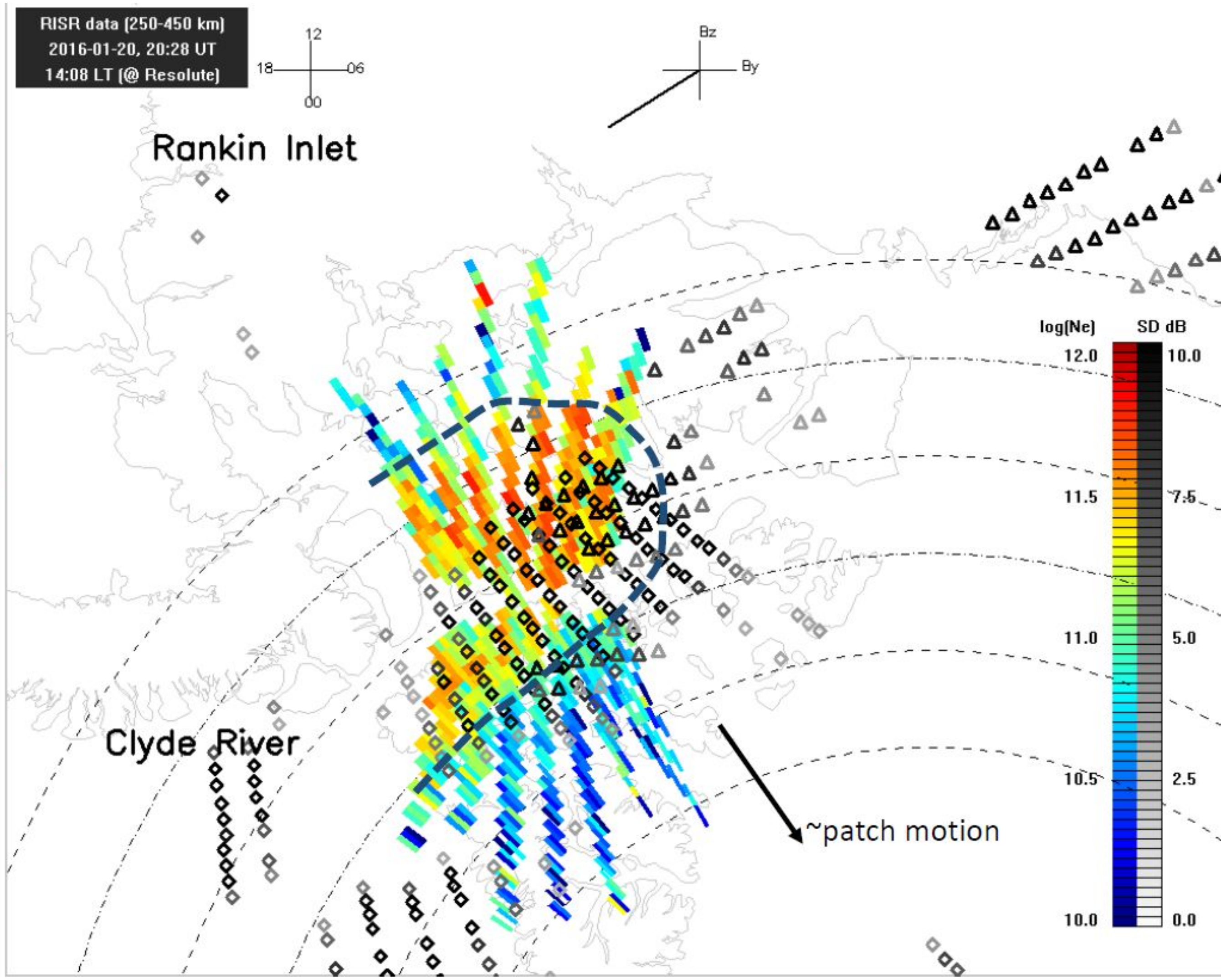

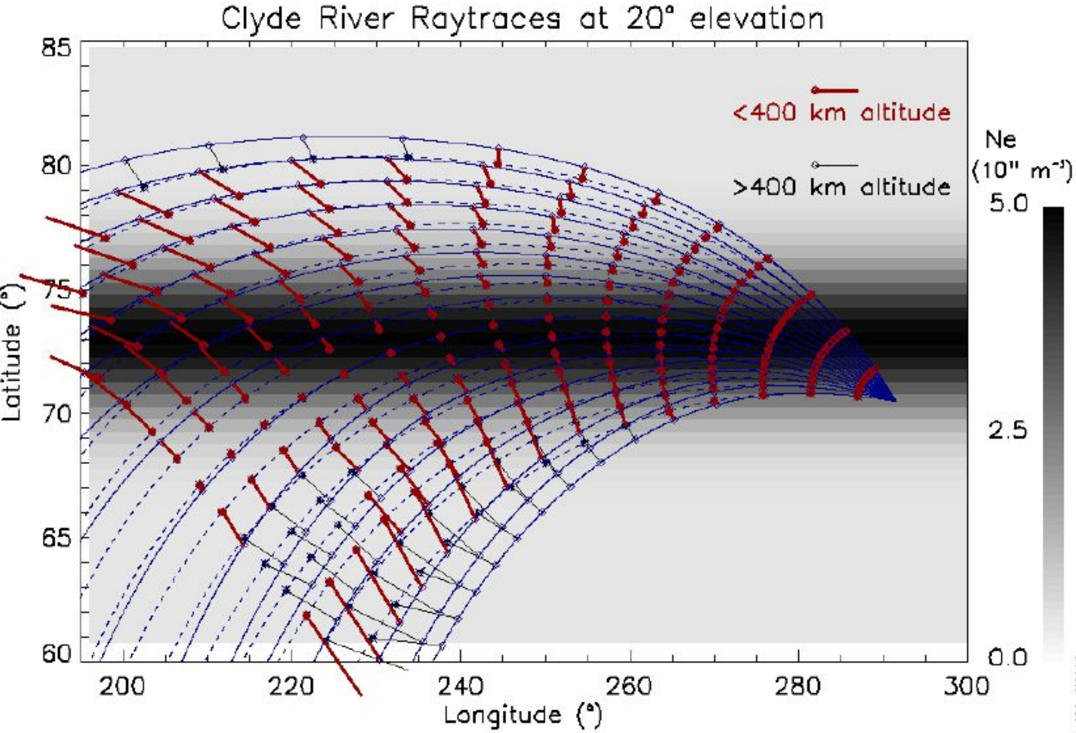

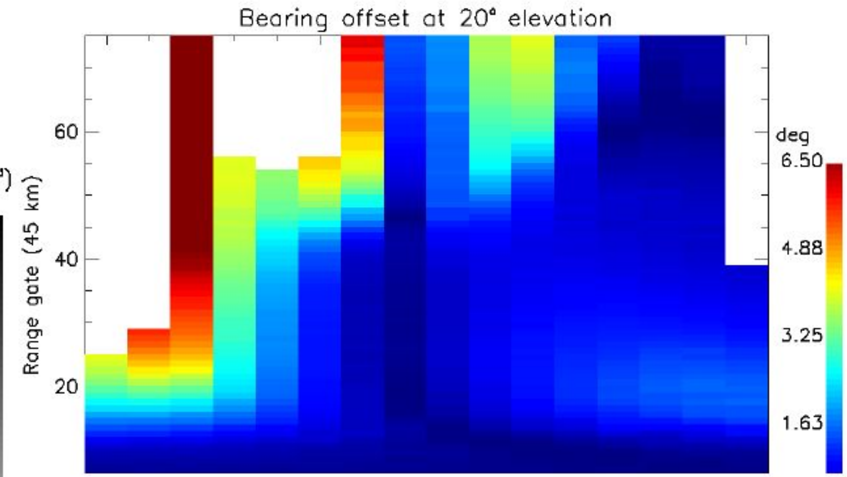

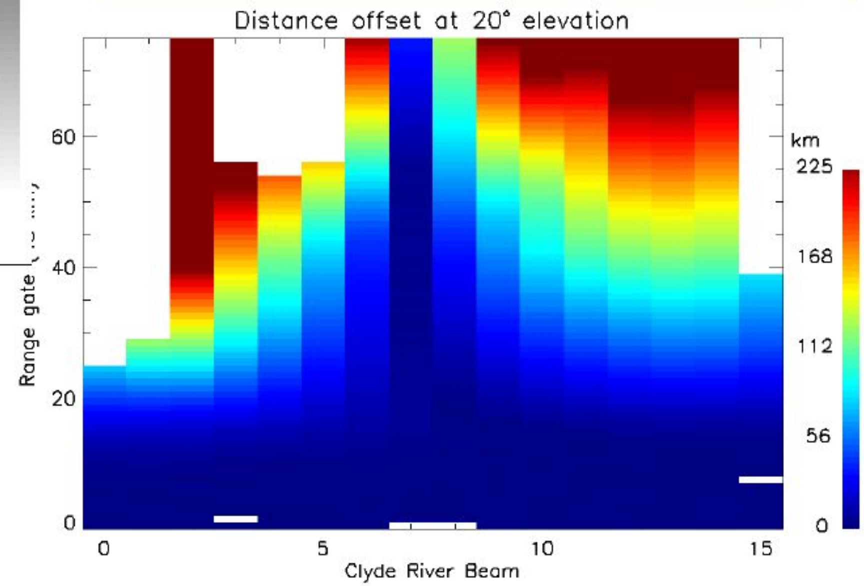

- Ray traces performed using modelled polar patch based on RISR measurements from previous slide (density and latitudinal width)
- Location and bearing of each range gate compared to similar ray traces without density gradient
- Bearing offset >6.5° for some beams at farther ranges (i.e., > 2 SuperDARN beams)
- Horizontal distance offset > 225 km for several beams (i.e., > 5 SuperDARN range gates)

Questions, Discussion
Please add your name to your comment.

Cheryl:What is the limit on spatial and temporal resolution necessary for relevant processes? How do we define the geoeffectiveness of the fine scale structure?

.

AGU sessions

SA004: Cross-scaling coupling and energy transfer in the magnetosphere-ionosphere-thermosphere system
https://agu.confex.com/agu/fm18/prelim.cgi/Session/54439

SA011: Modeling the polar ionosphere: from basic science to operations
https://agu.confex.com/agu/fm18/prelim.cgi/Session/50826